Title
Synthesis and Analysis of Novel Materials for Plastic Scintillators

Author
Kishpaugh, David

Publication Date
2017

Peer reviewed|Thesis/dissertation

UNIVERSITY OF CALIFORNIA

Los Angeles

Synthesis and Analysis of Novel Materials for Plastic Scintillators

A dissertation submitted in partial satisfaction of the requirements for the degree Doctor of Philosophy in Materials Science and Engineering

by

David Allan Kishpaugh

2017

ABSTRACT OF THE DISSERTATION

Synthesis and Analysis of Novel Materials for Plastic Scintillators

by

David Allan Kishpaugh

Doctor of Philosophy in Materials Science and Engineering

University of California, Los Angeles, 2017

Professor Qibing Pei, Chair

This work seeks improve gamma scintillation light yield of organic plastic scintillators in pursuit of an improved detection technology for radiological and nuclear material. The detection and tracking of such material in transit, especially across borders, is a critical concern to the national security community. Novel polymer systems and additives have been developed, synthesized, and characterized which achieve this end while maintaining the robust nature and ease of fabrication which are the hallmarks of plastic scintillators. The results have shown significant improvement in extrapolated light yield over commercial standards when characterized with photomultiplier tubes. Further analysis has also demonstrated the utility of these materials with solid state silicon photomultiplier type detectors. In pursuit of further gains in performance, a new energy harvesting material making use of developments in the field of

thermally activated delayed fluorescent compounds has been designed, synthesized, and characterized. The results from this work show promise and point to opportunities to make major increases in plastic light yield through further tailoring matrix and dopant materials.

The dissertation of David Allan Kishpaugh is approved.

Dwight Christopher Streit

Benjamin Joel Schwartz

Qibing Pei, Committee Chair

University of California, Los Angeles

2017

Dedication Page

This work is dedicated to the many people who have made it possible with their enduring support and guidance.

To my parents, Charlie and Karen Kishpaugh, and my grandparents, Donna and Allan Hochstetler, Allan Kishpaugh, and Hal and Sally Singley for their unending love, tireless encouragement, and lifelong contributions to my education.

To my many friends who supported me completely through all the struggles along the way – especially Danielle Casillas, Jesse Ko, Sing Mok, Christopher Roberts, Andrew Wong, Jennie Davidow, Emily Pittore, and Charming Yu.

And to those who have made this possible through their mentorship, both formal and otherwise – especially Dr. Brian H. Northrop, Dr. Richard Binzel, Dr. Donna Metz, Dr. Stewart E. Novick, and Dr. Andrea Roberts.

Table of Contents

List of Figures

List of Tables

Acknowledgements

This work could not have been accomplished without the contributions, consultations, hard work, and guidance of my Advisor, Dr Pei as well as the members of the scintillation group Jacob Hajagos, Chao Liu, Yi Chen, and Qi Chen.

In addition, the thoughtful commentary and time of my other committee members, Drs. Dwight Streit, Ioanna Kakoulli, and Benjamin Schwartz, was of great help and is much appreciated.

The work reported herein was performed with the financial support of the Domestic Nuclear Detection Office (DNDO), part of the U.S. Department of Homeland Security (DHS), under the Grant ID 2014-DN-077-ARI071-0. This work is also based on the use of instruments at the UCLA Molecular Instrumentation Center (MIC) that are supported by the National Science Foundation under equipment Grant no.CHE-1048804.

A portion of the work described herein is under revision for publication in the journal Nuclear Instruments & Methods in Physics Research A: Accelerators, Spectrometers, Detectors and Associated Equipment under the title *Applications of Fluorene Moiety Containing Polymers for Improved Scintillation Light Yield*. This work is reproduced in part here under the author's right to personal use in academic context.

Vita

2007	Bachelor of Arts, Chemistry and Physics
	Wesleyan University
2013	Master of Science, Materials Science and Engineering
	University of California, Los Angeles

I. Introduction

Radiation Detection

The proliferation of state and non-state actors with the ability to deploy nuclear devices at varying levels of sophistication is of serious concern to the international community. The use of nuclear material coupled with conventional explosives (a "dirty bomb") is particularly troubling given the relative ease of assembly and deployment and the prevalence of terrorist groups willing to do so. While the actual health and damage effects of such an unsophisticated weapon are debated,[1,2] the terrorizing effects are certain – particularly given strong public fears surrounding radiation. Countering these radiological threats requires improved control systems and better, more easily implemented detection technologies. In particular, there is a demand for improved portal monitors to interdict radioactive material in transit as it crosses borders and passes through ports. The magnitude of the search space is extraordinary - in 2013 total container traffic at United States' ports was in excess of 44.5 million twenty-foot shipping containers.[3] In 2015, the Port of Long Beach alone handled the equivalent of 7.2 million shipping containers.[4] Effectively screening an appreciable fraction of this cargo flow requires efficient, large volume detectors to be available at low cost and in large quantities. The economic costs of delays and false positives mean speed and reliability are essential.

Current portal monitoring technology is based on scintillators – materials which emit photons of visible light when exposed to other forms of radiation. To use such a material as a detector, the scintillator is coupled to an optical photon counter such as a photomultiplier tube, photodiode, or silicone photomultiplier. The light generated is captured by these counters and

converted into an electrical signal which can be processed to potentially determine the flux, energy, and type of radiation present.

Currently, commercial scintillators are primarily composed of either alkali halides or polyvinyl toluene plastic.[5] Alkali halides offer high scintillation efficiency and gamma ray spectroscopy, but have several drawbacks – e.g. high cost, rare materials, and poor scintillator ruggedness. Plastic scintillators suffer from lower efficiency, but can be more economically obtained in larger sizes and are less easily damaged by environmental conditions – ie: thermal shock or exposure to water.[5] The aim of this project is to improve the available scintillation materials by developing better plastic scintillator compounds, which will lead to more efficient, effective detection and neutralization of radiological threats while maintaining plastic scintillators price and durability advantage.

The "efficiency" of a scintillator is essentially its ability to convert the energy in a flux of radiation into measureable photons. The typical evaluation metric for this property is the "light yield" of a scintillator. Light yield is measured in units of photons produced per MeV of energy deposited [ph/MeV], although in practice the determination of this quantity usually relies on comparison to a known standard, for example Anthracene or Sodium Iodide. Consequently in the literature and here light yields are frequently reported as "78% of anthracene".

To understand the full scintillation process, it is critical to at least grasp the basics of energy deposition in the scintillator matrix. This requires an understanding of the forms of radiation which may elicit scintillation and their methods of interaction with the detector. There are four primary forms of radiation arising from nuclear processes - heavy charged particles (primarily α-rays), electrons (β-rays), electromagnetic radiation (x- and γ-rays), and neutrons –

with each form dissipating differently in matter. This leads to two primary consequences: 1) not every scintillator is optimized for the detection of every type of radiation and 2) the information conveyed can be different for each type of particle. For the purposes of radioisotope detection in the security context the radiation types may be roughly ordered from least to most useful as follows: alpha, beta, neutron, and gamma.

Alpha and beta rays are of little importance primarily because of their low mean free path through common shielding materials. Alpha rays in particular, due to their high mass and charged nature, are generally absorbed in a distance on the order of 10 cm in air. Beta rays are easily shielded by a reasonable layer of metal; even a few centimeters would suffice. Although these rays may be useful in medical or other imaging applications, in searching for contraband nuclear material it is desirable to employ a less easily foiled detection strategy.

Neutrons differ substantially from these first two forms of radiation due to their lack of charge. As a result, the primary interaction of a neutron with a scintillator is through neutron capture reactions with receptive species (in the case of thermal neutrons) or by generation of recoil protons and subsequent ionizations (in the case of fast neutrons).[6] The first mechanism requires the scintillator to be doped with isotopes susceptible to neutron reactions. The best candidates in terms of cross section are ^{6}Li and ^{10}B. Both have been incorporated into inorganic scintillators,[7–9] and clever synthetic strategies have been employed to reach usable doping levels of these isotopes in organic materials.[10–12] Both liquid and plastic organic scintillators doped with Boron-10 are available from Eljen Technologies.

One aspect of fast neutrons that is of special importance comes from their similarity in penetration depth to γ-rays. Differentiating the two events therefore requires detailed Pulse Shape Discrimination [PSD] analysis. However this extra effort provides information about the

relative presence of γ and neutron events which can lead to spectroscopic identification of an isotope. This is especially useful in security screening to assess the threat potential of a radioactive source. Several innocuous materials, for example concrete and bananas[1], have high, but harmless, radiation signatures. The ability to determine that these isotopes are the cause of a positive detection event and forgo further costly screening is of great utility in this context.

Neutrons are reasonably easy to detect and difficult to shield, providing a better option for radioisotope detection than alpha or beta rays. However neutrons are not emitted by all fissile materials, limiting their general use. Thus γ-ray electromagnetic radiation is the preferred means of analysis for threat detection. It is universally released by radioactive processes and requires thick heavy metal shielding – making concealment costly and impractical. This shielding difficulty, however, arises from the high penetration depth and low probability of energy deposition of γ-rays. As a result, detection is also more difficult. This is especially true for the less absorbent, lower Z elements found in plastic scintillators.

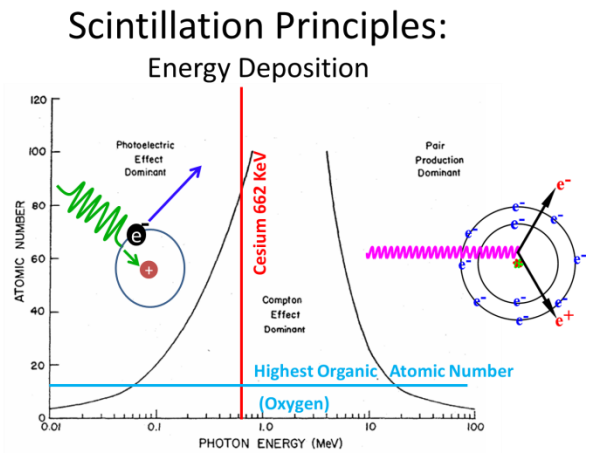

Figure 1 - The three energy deposition mechanisms dominant at different γ-ray energies and atomic numbers. The main γ-ray of ^{137}Cs and the highest atomic number found in most organic scintillators (Oxygen, 16) are marked.

The γ-ray/scintillator interaction is more complex than that of the other radiation types, with different energy deposition interactions dominating at different atomic numbers and over different energy ranges [Figure 1]. Of these three mechanisms – photoelectric effect, Compton Effect, and pair

[1] Bananas are very high in potassium which has a very high isotopic abundance of radioactive ^{40}K.

production – only the first two are of real importance at the energy levels and atomic numbers generally of interest. Pair production dominates in the higher energy regime well above twice the electron rest mass (~0.5 MeV). In pair production a gamma ray of sufficient energy is absorbed, and through coulombic interactions with the nucleolus, an electron and a positron are created. This process is exclusively effective for very high energy gamma rays.

In the low energy regime – roughly < 60 keV in organic materials – gamma ray absorption is dominated by the photoelectric effect which occurs when gamma rays are absorbed by a molecule and a core shell electron is ionized from that energy. In this process the entire energy of a gamma ray is deposited in the scintillator – making it is ideal for spectroscopy. This energy signal is easily recognized on the counts versus energy plot typically generated by a scintillation detector and is known as the Photopeak. It offers a unique isotope identifier by giving a value for the energy of the gamma emission of the source – rather than fractions of that energy deposited by the Compton Effect. Looking at Figure 1, it is clear that spectroscopy is limited in any organic scintillator (plastic, liquid, or crystalline) by the low atomic number of the elements present. If the detection of a photopeak is desired in these materials, special considerations must be employed. These will be discussed briefly later.

As noted, the Compton scattering mechanism dominates in the intermediate energy range and at the low atomic numbers found in purely plastic scintillators. With our research in organic scintillators we are primarily concerned with this effect. Like the photoelectric effect, Compton scattering occurs through the

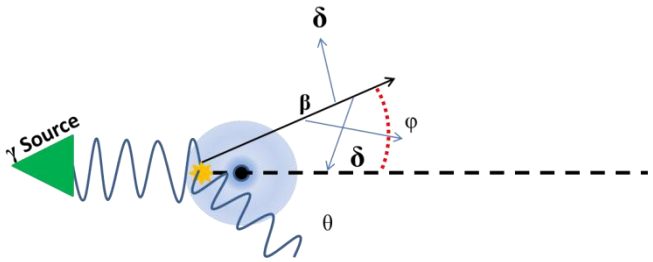

Figure 2 – Schematic of Compton scattering effect, the primary mechanism at work in plastic scintillators.

ionization of an electron by interaction with a gamma ray. However while the photoelectric effect results from the complete absorption of the gamma ray, in Compton scattering the interaction may take a range of energies from the gamma ray while the gamma ray itself is not absorbed but instead scattered to a new angle. The energy of the ionized electron is dependent on the change in wavelength of the β-ray, which is related to the scattering angle [Figure 2; Equation 1].

Equation 1

$$\Delta\lambda = \frac{h}{m_0 c}(1 - \cos(\theta))$$

After ionization the electron is effectively a β-ray, which interacts with the scintillator as a β-ray directly from a radioisotope source would – through coulombic interaction with inner and outer shell electrons which result in further ionizations as the beta ray dissipates its energy. These ionizations result in further emitted electrons (δ-rays) at lower energies, which in turn cause excitation in the scintillator matrix. The excitation bases through an energy cascade dependent on the type of scintillator and is then converted to photons through radiative recombination. The key fact about Compton scattering is that it never permits total energy deposition, thus making isotopic identification impossible purely on the basis of Compton Scattering.

Given that the Compton Scattering of γ-rays is the primary mechanism of energy deposition with which we are concerned, the goal of increasing a scintillators light yield must then come from one of two strategies – i) improving excitation harvesting to maximize the

energy from γ-ray interaction which is converted into radiative events; and ii) raise the probability of γ-ray interaction events. Because the γ-ray interaction probability is proportional to Z^4, the latter strategy requires the incorporation of high-Z additives to raise the collective gamma interaction cross section of the scintillator. A variety of work has been done on this topic – using heavy metals,[13,14] organometallics,[15–17] and nanoparticles,[18–20] to increase gamma interaction probability and create plastic scintillators with a photopeak. For this project we pursue the alternative approach – raising the number of photons produced per MeV of energy deposited [ph/MeV] in plastic scintillators. A brief history of scintillator development may be instructive for examining the path forward and is offered below.

Scintillator History

The discovery of x-rays in 1895 was accomplished with a glowing barium platino-cyanide screen. In the race to learn more about this phenomenon, other fluors coupled to photographic film were the primary tools for almost 5 decades - the most popular and long lived of these being $CaWO_4$ and ZnS. The discovery of the photomultiplier tube [PMT] in the 1940's opened the door to development the first scintillator detectors in the modern sense in 1948, which also coincides with the dawn of the nuclear age.[21,22] Thallium doped sodium iodide crystals [NaI(Tl)] were the first developed and since that time have represented the traditional gold standard of scintillation technology, exhibiting a light yield of 38,000 Photons/MeV and an excellent energy resolution of 6% under ^{137}Cs irradiation[23]. Attempts to improve on NaI(Tl) focused intensely on inorganics including alkali halides[24], silicates[25], oxides[16], and rare earth oxides[26] however only around the turn of the millennium[27] did $LaBr_3$(Ce) surpass NaI(Tl) as

the top performing commercial scintillator option – with a light yield of 63,000 Photons/MeV and a decay time of 16 ns (vs 250 ns)[23,27]. In Light Yield performance, inorganic crystals are the clear choice in scintillation technology, however there are practical complications. The materials are all hygroscopic and require handling and packaging under inert atmosphere to avoid damage. The requirement of crystal growth constrains cost of possible detectors; while the incorporation of rare earth elements adds cost and limits the production of these devices in high numbers. The continuing development of organic scintillators has led to materials which avoid these issues.

Organic scintillators typically take the form of aromatic compounds with high delocalized π-electron density – this offers more available energy transitions and in turn greater opportunity for secondary δ-rays to excite electrons and lead to radiative transitions. Organic compounds, composed of light elemental compositions, have lower gamma ray stopping power than denser alkali halide materials however there is a long history in the literature of efforts to improve this feature with additives[13,18,19,28,29]. The first organic scintillators, developed circa 1948, were crystalline polycyclic aromatic hydrocarbons such as anthracene and naphthalene[30]. While the light yield of 20,000 Ph/MeV for Anthracene is respectable, these organic crystals do not produce a gamma photopeak, and suffer similar stability and size limitations as inorganic crystals. Only the excellent response speed of these materials recommends them over top inorganics.

Liquid scintillators based on alkyl benzenes such as toluene and xylenes with dissolved fluorescent molecules to promote radiative recombination were developed to overcome scalability and cost issues. These mixtures show good energy transfer via molecular migration,

acceptable light yield [eg: 78% of anthracene for the commercially available EJ-301 formulation][31], and are easily manufactured. However, they suffer from obvious drawbacks associated with encapsulation, deployment, and flammability that have prevented wide-spread adoption. Plastic scintillators, composed of similar solutions of alkyl benzenes with fluorescent molecules in the polymer form, aim to capture the advantages of liquid and crystalline scintillators in the same material without their respective drawbacks.[32]

Initially described in the 1950's,[32] plastic scintillators are now widely available commercially at a light yield of roughly 64% of anthracene[33] and are generally polystyrene [PS] or Poly(vinyl toluene) [PVT] matrices with various included dopants. The much greater volume fraction of matrix material versus dopants means energy deposition primarily occurs within the polymer matrix. The emission color is tuned by the selected dopants and generally chosen to match the deep blue sensitivity of coupled photomultiplier tubes. As discussed, the goal of such materials is the incorporation of the most desirable properties of liquid scintillators without the concomitant difficulties. In that sense plastic scintillators are a success - they are low cost, scalable to large size, offer virtually unlimited form factors through molding and machining, are highly durable, have no health or flammability risks, and already offer a suitable technology for portal monitoring applications. However, even the best plastic scintillators are inferior to liquids in performance to say nothing of anthracene or their fractional light yield compared to the top inorganic crystals. The aim in this project is to improve the light yield of plastic scintillators by exploring novel matrix and fluor compounds. As discussed, the approach is focused on improved capture and radiative emission of energy deposited in γ-ray impact events, not on increasing the raw number of γ-ray events through additives.

Scintillator Principles and Development

An understanding of the mechanisms underlying the scintillation process is essential to evaluating materials for scintillator potential. Here we summarize from above how energy is absorbed in a scintillator; then explore in greater detail the conversion and emission of that energy as a photon – focusing on the material requirements at each step.

Due to their low effective mass, energy deposition in organic materials is dominated by Compton Scattering for gamma rays of roughly 60 keV to 11 MeV. This process generates an ionized electron – effectively a β-ray – in the matrix and scatters the γ-ray. The β-ray subsequently ionizes electrons at lower energies through columbic interactions to form δ-rays, which create excited states in the polymer matrix. In contrast to massive particles, electromagnetic radiation is absorbed or scattered in single events and its high penetration in plastics means γ-rays are unlikely to interact more than once within a scintillator sample. A consequence of these effects is that above the energy threshold where Compton Scattering is dominant virtually no γ-ray/scintillator interactions result in the deposition of the total available energy of the γ-ray – and thus no photopeak is visible when using organic materials. In the absence of high-Z sensitizers to improve the probability of γ-ray absorption via the photoelectric energy deposition process, the main requirement for a matrix is the efficient use of the energy that is deposited.

Efficient conversion of the matrix excitation into photons proceeds in two steps – 1) transfer to fluorescent dopants and 2) dopant radiative relaxation. In matrices with inherently high fluorescence, emission will come directly from the matrix; however in any practically sized scintillator self-absorption will severely limit the contribution of this emission to the observed

light yield. Consequently, a matrix possessing a high Stokes shift is desirable and fluorescent dopants still play a key role to limit detrimental self-absorption. The second step in this process obviously requires excellent quantum efficiency from the fluor. The primary additional requirement for fluors is sufficient solubility. Although used in very dilute solution of at most a few wt% for primary fluors, solubility in more rigid solid polymers can still be a challenge without appropriate fluor design. The first step in the energy conversion process is more complex.

In scintillators, there are potentially three energy transfer mechanisms operating – exciton migration, radiative transfer, and long range dipole transfer. Exciton migration is expected to be supported by the delocalized π electron system of the conjugated matrix materials used in organic scintillators. Radiative and long range energy transfer both require spectral overlap between donor and acceptor molecules. In polymer systems the relevant donor bands may be either those of the respective monomer or of excimer structures formed in the polymer.[34] Vinyl toluene possesses poor quantum efficiency which limits radiative transfer occurrence to excimer bands rather than direct monomer emission. As a result any energy deposition must pass through an excimer state – either by formation at the current site or migration to specific excimer sites in the polymer – prior to transfer to a fluor.[34] Both processes have non-unity efficiency, resulting in potential energy loss. This suggests that while high radiative quantum efficiency is not a necessity of the matrix material, improving it without sacrificing other factors is a method to improving energy transfer and light yield.

To further expand the available energy harvested without increasing the probability of deposition, we target the triplet states generated by γ–rays. Statistically, triplet states make up

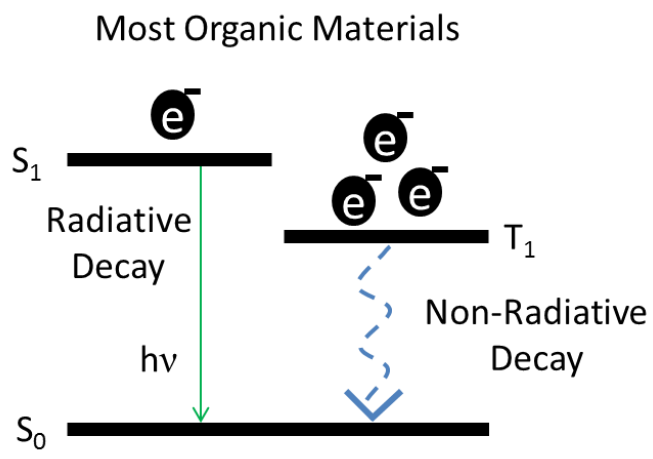

Figure 3 – In most common organic materials non-radiative decay occurs for excited electrons in the Triplet state as a consequence of the spin-forbidden transition to the ground state preventing radiative decay.

75% of those states formed from an ionization/excitation event. However, in most organic materials such as the polymer matrix and fluorescent dopants, triplet states produce very few radiative events at room temperature due to the spin-forbidden ^{1}T-^{0}S transition to the ground state [Figure 3]. Instead these electrons in excited triplet states return non-radiatively return to the ground state through thermalization. Without access to these triplet state excitons, the efficiency of a device is limited to 25%. Improved harvesting efficiency of these triplet states into photons for detection could improve light yield significantly – to a first approximation up to 4 fold, although practically lower when considering other effects.

Given the potential light yield gains, there is a clear motivation to find materials and methods to overcome this limitation. Several mechanisms have been proposed and studied, generally in relation to organic light emitting diode [OLED] devices. The three primary mechanisms are taking advantage of Triplet-Triplet Annihilation [TTA], incorporation of phosphorescent dopants, and use of thermally activated delayed fluorescence [TADF] materials. All three methods are briefly described in the next section.

Triplet State Harvesting Methods

Triplet-Triplet Annihilation

Triplet-triplet annihilation requires encounters and recombination between excited triplet states leading to one singlet excited state and one singlet ground state. This is shown symbolically in Equation 2 and schematically in Figure 4.[35] TTA is a bimolecular process, requiring a high density of excited triplet states and long enough lifetimes to permit their diffusion and interaction. These requirements make the TTA process much more important in OLED devices and scintillators than in contexts where photoexcitation is the dominant process. In OLED devices the driving currents lead to a high density of excited electrons. In scintillators the density of excited states is also be high due to the high energy of the particles interacting in the material and the short distance over which energy is dissipated from incident radiation.

Equation 2 – S_x^v denotes a vibrational excited state.

$$T_1 + T_1 \rightarrow S_1^v + S_0^v \rightarrow S_1 + S_0$$

After annihilation, the excited singlet state created may fluoresce through radiative decay as with a singlet excition derived directly from incident radiation. However this fluorescence will be delayed formation time of the excited singlet state via triplet-triplet annihilation. Light from this process is known as P-type Delayed Fluorescence[2]. This delay is used to distinguish neutron and γ-ray events in the PSD method described above by virtue of their different rates of

[2] "P-type" comes from pyrene, the molecule where this was first observed, not from "phosphorescence".

formation of triplet states.

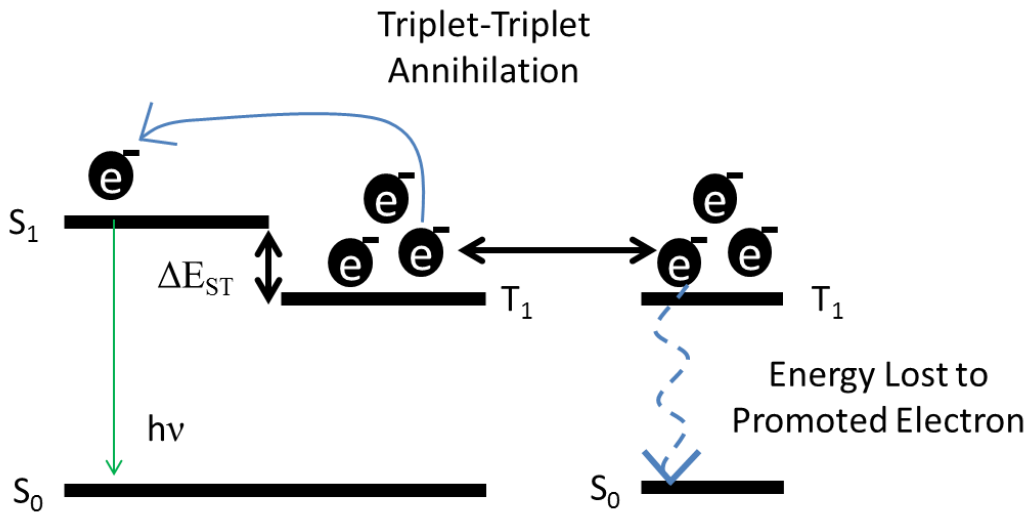

Figure 4 – In Triplet-Triplet Annihilation two electrons in the T_1 state on different molecules interact to transfer their energy to one of the electrons. This electron is promoted to the S_1 state while the other electron goes into the S_0 state. TTA requires the ΔE_{ST} to be less than the T_1 energy. The process conserves spin.

In OLED devices, TTA appears to be an important contributor to light yields in excess of the theoretical efficiency maximum of pure singlet emission.[36] However it is not the most efficient process by its very nature – that is, turning two excited states into one excited state – which leads to a maximum theoretical quantum efficiency of 62.5%.[37] For this reason, the primary focus of this work has been on phosphorescent and thermally activated delayed fluorescence dopants.

Organometallic Phosphorescent Dopants

Organometallic phosphorescent dopants, frequently organoiridium complexes, overcome the spin-forbidden ^1T-^0S transition through increased spin-orbit coupling. In spin-orbit coupling,

magnetic interactions between electron motion and the electron's spin magnetic moment cause the lowest lying triplet state to contain contributions from singlet states.[35,38] These contributions relax the spin selection rules and give the triplet state enough singlet character to enable optical transitions and raise the radiative relaxation rate (k_r) from the triplet state.[35] The relative contributions of singlet states is dependent on the difference in energy between the states involved.[35] In general, an increase in k_r, leads to increasing phosphorescent quantum efficiency.[38]

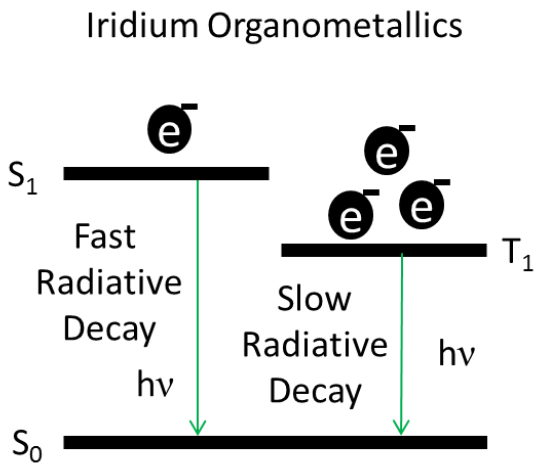

Figure 5 – Organometallic complexes with heavy metal center ions can be designed to exhibit high levels of phosphorescence. This is due to the spin-orbit coupling which occurs around the metal ion, permitting radiative ^1T to ^0S transitions.

Organometallics using with this property have the theoretical potential to access all the available triplet energy deposited in the scintillator matrix and consequently have been an area of interest in this work, with the focus being primarily on material design to allow dispersal of otherwise low solubility dopants in the polymer melt.

Thermally Activated Delayed Fluorescence

An alternative triplet harvesting approach is the use of another class of materials which exhibit E-type[3] delayed fluorescence, also known thermally activated delayed fluorescence, or TADF.

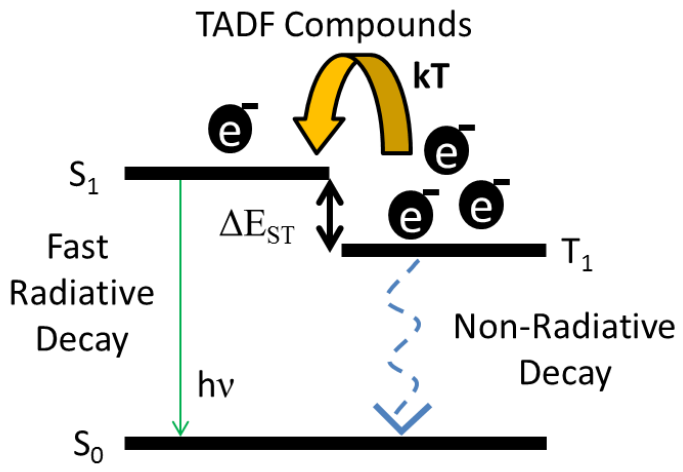

Figure 6 – A schematic depiction of the TADF process. Electrons in the triplet state are thermally promoted into the first singlet excited state over the low energy barrier through reverse intersystem crossing.

The TADF process occurs in fluorescent molecules possessing a very small ^1S-^1T energy gap (ΔE_{ST}), which permits up-conversion from triplet to singlet state from environmentally available thermal energy [Figure 6]. The process leads to a delayed emission with respect to normal fluorescence as a consequence of the additional transfer step. Given the thermal energy promotion mechanism for the triplet to singlet transfer, the minimization of ΔE_{ST} is critical, and the achievement of this through molecular design will be discussed below. TADF has been successfully used to boost efficiency in OLED devices.[39–41] and we propose that it can be utilized to improve the harvesting of deposited energy through collection of triplet states in scintillators. Unlike TTA, the TADF process is unimolecular and offers the potential for greater efficiency by reducing the two to one conversion of excitons seen in TTA.

[3] This name again comes from the compound of original discovery, the dye eosin.

Material Design

Matrix and Fluor Design

Having now developed a strong understanding of the scintillation process, a description of the types of materials of interest and the structural demands placed upon them can be constructed. In terms of the matrix compositions, materials with good performance characteristics should be conjugated structures with high electron density thereby raising the probability of electron interaction with gamma rays and the ionized electron which results from Compton Scattering. In addition, a desirable matrix material should also possess high luminescent quantum efficiency, large stoke shift, and high triplet energy. These properties respectively impart high rates of radiative recombination, low self-absorption losses, and the opportunity to harvest triplet excitons for visible light photons. Many of these characteristics are common requirements in OLED materials and for this reason we draw inspiration from this field in working to improve scintillators.

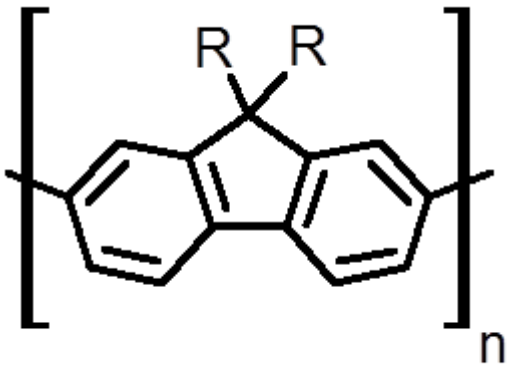

Figure 7 – The fluorene moiety of a generic polyfluorene polymer.

OLED materials also possess a practically important characteristic – their emission spectra are by necessity in the visible range. For scintillator materials the most desirable range of emission is in the deep blue – which tends to match well with existing PMT detectors – or the green – which is more suitable for solid state detectors.

Polyfluorene and its derivatives are well-known compounds in blue OLED devices. Fluorene structures are also utilized in oligomer form and as a moiety in larger π-conjugated molecules.[42–45] The attachment of other moieties to the base fluorene units is used to alter energy levels to a more favorable configuration for OLED devices. In the scintillator application the main difference is our requirements for a curable monomer to create the polymer matrix replacing PVT. Consequently we aim to synthesize a fluorene-based structure attached to polymerizable side groups. Another important aspect of our molecular design is a desire for high solubility, low crystallinity, and low melting point. An increased amorphous character to the matrix material promotes solubility of dopants used as fluors. The low melting point makes molding scintillators out of a melt simple and reduces the risk of component degradation associated with higher temperatures. This is in contrast to OLED processing strategies, which frequently involve deposition techniques designed to deal with lower quantities of polyfluorene and other light emitting compounds. In these environments, solubility is not a primary concern. For our purposes we have generally sought to lower melting points and improve dopant solubility with addition of crystallization inhibiting aliphatic chains to the periphery of our matrix materials (eg: substituting the –R groups in the 9 position in Figure 7). Chapter II will explore the structures used to achieve these qualities, the synthetic methods employed to realize the final product, and the fabrication of scintillator samples from these synthesized monomers. First, however, the specific design concerns of the triplet harvesting dopants will be addressed.

Triplet Harvester Considerations

In designing triplet exciton harvesting dopants, solubility again becomes a crucial obstacle in our design. In contrast to fluorescent dopants which can be dispersed at ~ 1 wt% in

the scintillator matrix, dopants intended to access triplet exited states must reach much higher loadings.[38,46,47] This is a consequence of the difference between triplet and singlet excited state energy transfer in mechanism and effective range. Any energy transfer from an excited donor molecule to an acceptor molecule occurs along one of three pathways – 1) Radiative transfer, 2) Förster transfer, or 3) Dexter transfer. In a system of one type of donor and acceptor molecules, one process frequently dominates. Although only radiative energy transfer involves the explicit emission and absorption of photons, all three require spectral overlap between the donor emission and acceptor absorption. In Förster transfer, the overlap integral is a mathematical expression of the transitions moments of the donor and acceptor while in Dexter transfer it is related to their wave function overlap – both properties play a critical roles in the respective mechanisms.

The radiative pathway is obviously closed for triplet excitons in our system due to their primarily non-radiative decay. In addition, spin conservation prohibits triplet-triplet excited state transfer through Förster transfer. This mechanism, also known as resonance or induced dipole energy transfer would require spin forbidden transitions in both donor (D) and acceptor (A) molecules, as seen in Equation 3.[35]

Equation 3

$$^{3}D^{*} + {}^{1}A \rightarrow {}^{1}D + {}^{3}A^{*}$$

As a result, all triplet-triplet transfer must proceed through Dexter transfer which occurs when the excited electron on D* moves onto A through the overlap of their electron clouds while an electron from A is exchanged back. This electron exchange operates under different spin conservation rules due to the orthogonality of the electron's spin wave functions.[48,49] Thus as

long as the total spin of the combined system is conserved, the transfer is allowed. In other words, a final state where the spin of D* and A* and the spin of D and A are identical is permitted.[48]

In the scintillator context, the key difference between Förster and Dexter energy transfer is the effective range. Because the Dexter process requires electron cloud overlap, the rate falls off exponentially with the separation distance, R, between the molecules involved. Förster transfer, however, is proportional to R^{-6}, and can be effective up to 10 nm away while radiative transfer can operate over even longer distances.[35] Because R is dependent on the concentration of the acceptor molecule in the solution (i.e.: the polymer), the difference in effective radius for transmission of singlet and triplet states means a much greater concentration of triplet acceptors is required to effectively gather triplet excited states from the donor. From a material design perspective then, the ability to disperse triplet harvesting dopants in high concentrations is critical to their success. To achieve this we considered incorporation of aliphatic chains and co-polymerizable groups in our organoiridium fluors. The TADF materials explored may be a superior option to heavy metal complexes for triplet harvesting due to their inherently better compatibility in organic materials. Starting from promising TADF compounds in the literature, we sought to synthesize an analogue which retained the functional core and added peripheral functionality to improve solubility and increase the achievable loading in plastic scintillators.

TADF Design

Beyond solubility, TADF molecules require specific design criteria to achieve the precise behavior desired. The mechanism of TADF clearly requires a small ΔE_{ST} since, as Dias et al. note, the intensity of E-Type Delayed Fluorescence is "directly proportional to the energy gap between the triplet and singlet states".[39] This gap is in turn equal to twice the electron exchange energy (J) of the unpaired electrons in the singlet and triplet excited states which is determined from Equation 4.[50]

Equation 4

$$J = \iint \varphi_L(1)\varphi_H(2)\left(\frac{e^2}{r_1 - r_2}\right)\varphi_L(2)\varphi_H(1)dr_1dr_2$$

The key portion of Equation 4 is the integral over ϕ_L and ϕ_H, which represents the overlap of the HOMO and LUMO wave functions. From this equation it can be deduced that a reduction in the HOMO/LUMO overlap within the molecule will lead to improved TADF.[50]

Minimizing the overlap is accomplished by spatially separating the two orbitals and thus TADF materials frequently possess a "core" and "wing" intramolecular donor-acceptor structure [Figure 8] with the LUMO acceptor orbitals isolated on the core and the HOMO donor orbitals isolated on the wings. The twisted nature of the wings with respect to the core as a result of steric hindrance also misaligns the orbitals and improves separation. In addition to lowering $\Delta E_{ST,}$ careful tailoring of the orbitals through this method gives a strong intramolecular charge transfer character to the excited singlet and triplet states. As a result, TADF may even occur at high

efficiency with a ΔE_{ST} > 300 meV, despite a room temperature kT value of 25 meV – as long as both donor and acceptor triplet levels are higher than the charge transfer state.[39]

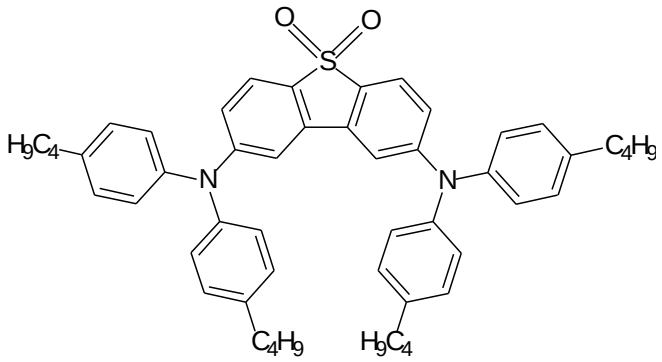

Figure 8 – Example TADF structure exhibiting the special separation of the HOMO (donor) orbitals on the wings and the LUMO (acceptor) orbitals on the core.

These orbital concerns are not the only structural considerations for TADF molecules. Other factors, including the solvent or solid environment and the precise attachment points between the core/wing structures can also impact the properties of these materials.[51] To develop TADF compounds we rely primarily on literature structures of TADF materials as a starting point, rather than deriving potential candidates from computational studies (which is a route other groups have taken). Our modifications have taken the form of improving solubility as per the requirements described above although further structural alterations have been necessitated as will become obvious.

Radiation Damage in Scintillator Materials

The basis of radiation detection by scintillation is the deposition of energy from ionizing radiation into the detector material. The clear consequence of this is the potential for damage to accumulate in the detector – in particular plastics are subject to defect formation from ionization, loss of hydrogen content, and formation of free radicals. These defects result in quenching sites, which have the effect of reducing light output of the scintillator. The behavior of plastic scintillators when accumulating damage is dependent on the particular type of base material, the incident radiation type and dosage, and the atmospheric composition.

Radiation sensitivity of polymers is strongly dependent on the functional groups present in the polymer and with the correct dopant choice derives more from the matrix composition than damage to the dopants.[52,53] Fortunately, as noted by Reichmanis, aromatic groups have been shown to "give significant radiation resistance to organic molecules".[54] Other structures, such as isolated carbon double bonds, halogens, and peroxides are particularly sensitive.[54] In general there are three types of radiation derived changes to polymer structure – crosslinking, scission, and coloring. Scission, the splitting off of molecules from the polymer chain, leads to reduced molecular weight and has a particularly deleterious effect on performance through the formation of small molecules, especially gasses such as H_2 and CO_2. The resulting gasses may be trapped in the matrix leading to crazing and cracking with reduces the light transmission of the polymer and the light yield of the scintillator.[54] Radiation induced coloring will also reduce a scintillators light yield through a loss of transparency, however the primary polymers which exhibit this property are polyacrylonitrile and PVC.[54] In addition, the presence of oxygen is correlated with increasing damage to the polymer matrix.[55]

The studies of degradation behavior in polymers have been made with a focus on the performance of scintillators in the context of high energy physics experiments. These environments are notable for exposing scintillators to high radiation doses or ion bombardment.[53,56,57] Consequently these detectors have the shortest lifetime. Indeed, studies generally show a trend of little notable loss of light yield below a threshold dosage, followed by a fall of in efficiency insensitive to the dosage rate.[52,55,57] In context of portal monitoring, the scintillator lifetime should not be appreciably affected by dosage. In principle a detector should be receiving very small doses of radiation; and in practice detection of a large does is worth the loss of a detector. As a result, we make no effort to study the damage in our detectors and could not with the radiation sources available to us.

II. Synthesis and Monolith Fabrication

Background

Our matrix material target, 2,7-bis{2'-9',9'-bis[(2''-ethylhexyl)-fluorenyl]}-9,9-bis(4'-vinylbenzyl)-fluorene, dubbed TFS, is shown in Figure 9. Key features of our material are the trimer fluorene structure, the aliphatic chains, and the styrenyl moieties. The trimer structure is responsible for the photophysical properties of TFS (e.g. the blue fluorescence). The other aspects effect how the compound is processed. The aliphatic chains serve to lower the melting temperature, increase the solubility of dopants, and generally give the material an amorphous character. The styrenyl moieties are responsible for the

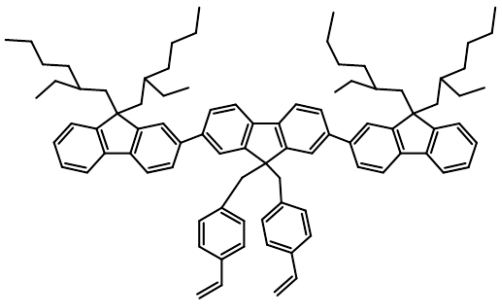

Figure 9 – Structure of TFS.

curable nature of the material, allowing for its incorporation into polymer devices. For cost and convenience, synthesis of the matrix material should require as few steps as possible and be scalable to generate large quantities in a single batch. We successfully synthesized TFS in high yield in four steps from commercial materials – using 2-bromofluorene and 2,7-dibromoflurene as key starting points. In addition we synthesized a fluor candidate, 4,7-bis{2'-9',9'-bis[(2''-ethylhexyl)-fluorenyl]}-benzo[c]-1,2,5-thiadiazole [FBtF], which proved to be a good candidate for pairing with our matrix material. Figure 11 shows structure FBtF and the similarity in structure to TFS which improves solubility in the matrix.

Monolith fabrication should ideally be accomplished in a short time frame and at low temperatures. Frequently, patented industrial processes for PS and PVT based scintillators span many days to weeks and require curing under vacuum with complex temperature ramping. Trials performed on our samples have shown that complex, high temperature cycling has a deleterious effect on sample quality. We attribute this effect to more rapid curing undergone by TFS and the effect of cross linking on the polymerization process. As a result our samples are cured in 24 hours at relatively low temperatures.

TFS was originally viewed as a replacement matrix material for PVT, however because it is a solid at room temperature, processing TFS into a monolith is very difficult. To counteract this, a range of TFS and vinyl toluene [VT] copolymer compositions were explored to determine an optimal composition. Addition of the liquid VT monomer helps dissolve TFS and create a homogenous mixture before the melt sets. Above 60 wt.% TFS, successfully formulating transparent monoliths is very difficult to do consistently.

Several alternative host materials were also synthesized and explored to varying degrees. Compounds based on triphenylbenzene and triphenylamine were synthesized for use by other groups while a fluorene dimer based compound 2-{2'-9',9'-bis[(2''-ethylhexyl)-fluorenyl]}-9,9-bis(4'-vinylbenzyl)-fluorene (known as DFS, Figure 10), was analyzed in house but demonstrated less promising results than TFS.

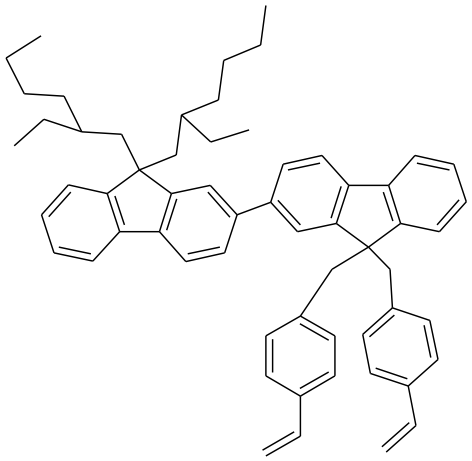

Figure 10 – Structure of DFS, one of several matrix materials explored in this work.

DFS is the dimer version of TFS. It lacks one of the ethylhexyl functionalized side fluorene moieties possesses a larger bandgap, lower wavelength emission due to the reduced conjugation of the molecule. This permits pairing with deeper blue fluors such as 2,5-bis(5-tertbutyl-2-benzoxazolyl)thiophene (BBOT). The lower wavelength emission allows for blue shifting the scintillator emission to more favorable wavelengths with respect to PMT detectors. In addition, DFS also exhibits a lower melting temperature (50-53^{o}C) than TFS (65^{o}C) and consequently could be cured at lower temperatures which may be an advantage. Exploration of DFS/VT copolymer mixtures was undertaken, however results proved to be less promising than TFS data when adjustments for spectral sensitivity were taken into account.

Experimental

All solvents used were ACS grade. Where used, dried tetrahydrofuran was freshly distilled over sodium benzophenone. Water work ups were performed with deionized water. Structures were verified by proton NMR using a Bruker AV 400. Photophysical characterization of prepared and commercial compounds in solution was done using a Photon Technologies International Quanta Master 4/SE with a Xenon arc lamp and a Shimadzu UV-1700 PharamSpec UV-VIS spectrometer.

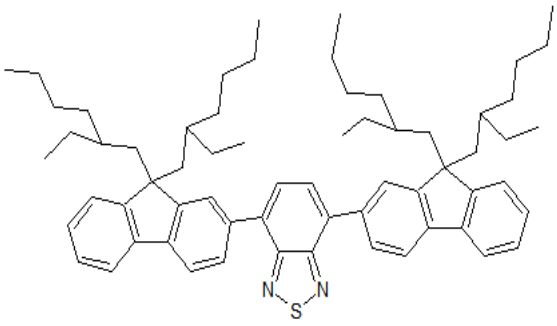

Figure 11- Structure of FBtF.

Synthesis of TFS

Scheme 1 – Diagram of synthesis of a novel fluorene based monomer.

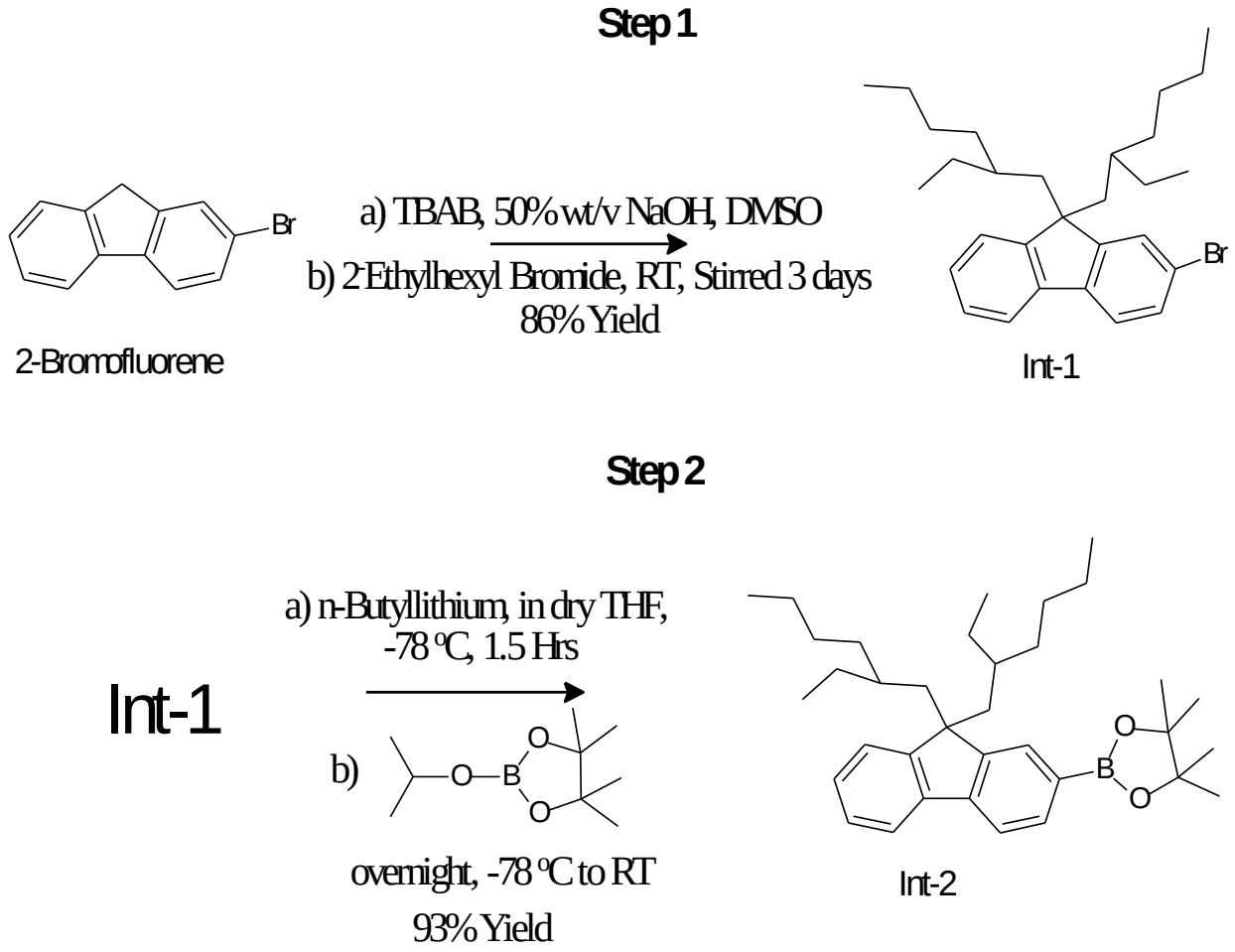

Step 3

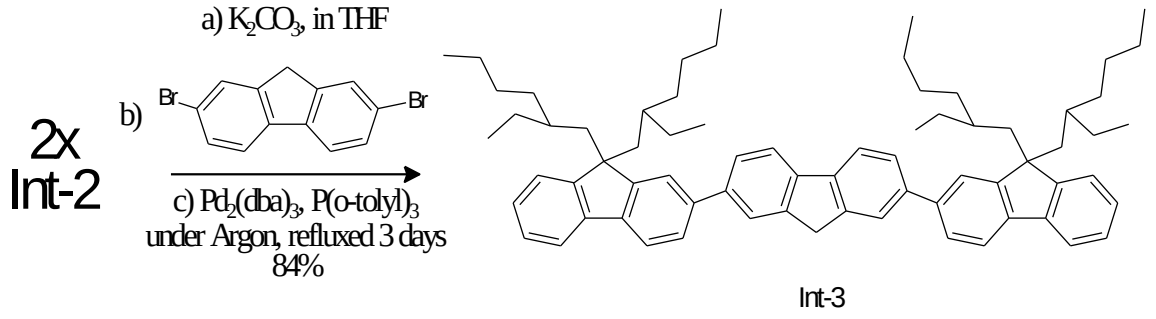

Step 4

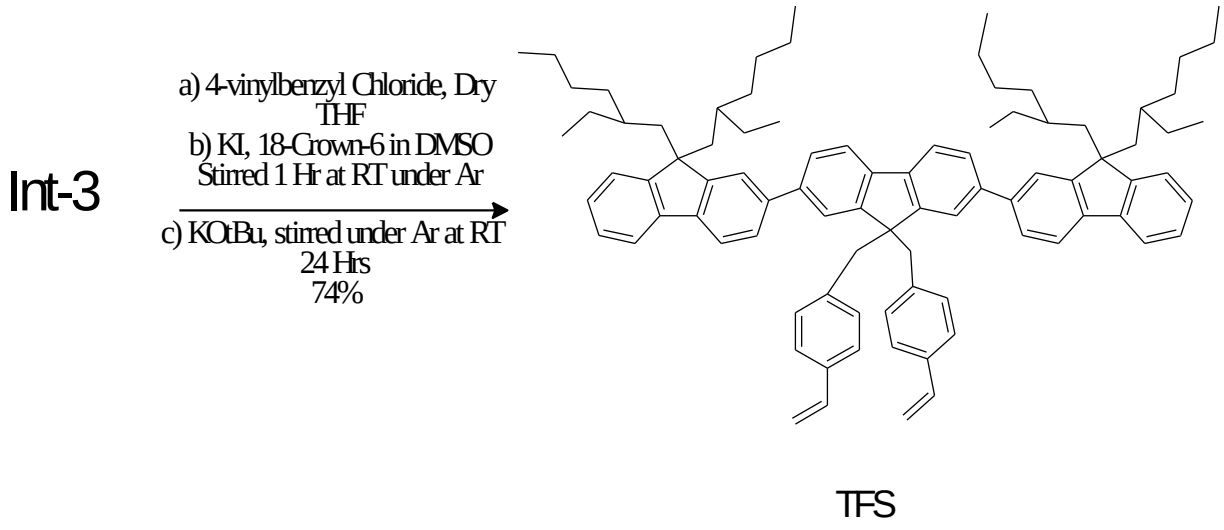

2-bromo-9,9-di(2-ethylhexyl)-fluorene [Int-1]

In a round bottom flask 13.71 g (55.9 mmol) 2-bromofluorne and 0.144 g (0.45 mmol) tetra-n-butylammonium bromide were dissolved in 100 mL dimethyl sulfoxide. To the mixture, while stirring, were added 23.15 mL of 50% wt/v NaOH and 29.84 mL (168 mmol) 2-ethylhexyl bromide. The reaction mixture was stirred 2 days at room temperature.

The reaction mixture was poured into water, quenched with 50 mL 2 M HCl, and extracted with diethyl ether. The combined organic layers were washed with water, dried over

magnesium sulfate, filtered, and concentrated by rotary evaporator. Excess ethylhexyl bromide was removed from the crude product via vacuum distillation at 1.3-1.5 torr. After distillation, the crude product was purified by flash column using hexane as eluent to collect 22.60 g of pure 2-bromo-9,9-di(2-ethylhexyl)-fluorene. The reaction proceeded in 86% yield.

2-[9,9-di(2'-ethylhexyl)-fluoren-2-yl]-4,4,5,5-tetramethyl-1,3,2-dioxaborolane [Int-2]

A round bottom flask was charged with 22.01 g (46.9 mmol) Int-1 under Argon. The compound was dissolved in 115 mL dry tetrahydrofuran. The solution was cooled to -78° C and stirred. To the stirring solution were slowly added 23.44 mL (58.6 mmol) of 2.5 M n-butyllithium in hexanes. The mixture was stirred for 2 hours at -78° C. To the reaction flask was added 24.42 g (131.3 mmol) 2-isopropoxy-4,4,5,5-tetramethyl-1,3,2-dioxaborolane. The reaction was stirred overnight and allowed to come to room temperature.

The reaction mixture was poured into water and quenched with 75 mL 2N HCl. The solution was extracted with diethyl ether. The organic layers were collected and washed twice with water and once with brine, then dried over magnesium sulfate, filtered, and concentrated by rotary evaporator.

The product was adsorbed on celite powder and purified in on a silica gel dry vacuum column in a solvent system from 1:0 to 6:1 hexanes:ethyl acetate. The purification yielded 22.60 g of pure product in 93.3% yield.

2,7-bis{2'-9',9'-bis[(2''-ethylhexyl)-fluorenyl]}-fluorene [Int-3]

In a three arm flask, 22.22 g (43 mmol) of Int-2 and 6.97 g (21.5 mmol) 2,7-dibromofluorene was dissolved in a solution of 210 mL tetrahydrofuran and 64.5 mL potassium carbonate in 2 M aqueous solution . To the solution were added 0.295 g (0.32 mmol) tri(dibenzylideneacetone)dipalladium(0) and 0.393 g (1.29 mmol) tri(o-tolyl)phosphine. The mixture was degassed thoroughly by freeze-pump-thaw, placed under Argon, and refluxed for 3 days at 90°C.

The reaction was removed from heat and extracted with diethyl ether. The collected ether was washed with water and brine. The organic layers were dried over magnesium sulfate, filtered, and concentrated by rotary evaporator to collect a crude product which was purified by flash column, using a 20:1 hexanes to dichloromethane eluent system. The solvent system was ramped to 18:1 and then to 15:1 over the course of purification. A final mass of 17.9 g was recovered for an 84% yield.

2,7-bis{2'-9',9'-bis[(2''-ethylhexyl)-fluorenyl]}-9,9-bis(4'-vinylbenzyl)-fluorene [TFS]

In a round bottom flask, 17.9 g (19 mmol) of Int-3 was dissolved in 250 mL freshly distilled tetrahydrofuran. The solution was stirred and flushed with argon for 15 minutes while cooling to room temperature. A solution of 1.37 g (5.2 mmol) 18-Crown-6 and 1.45 g (8.7 mmol) potassium iodide in roughly 50 mL dimethylsulfoxide was prepared and sonicated about 20 minutes, then flushed with Argon. The solution was added to the stirring solution of Int-3. To the mixture was added 9.27 g (60.7 mmol) 4-vinylbenzyl chloride. The reaction mixture was

stirred under argon for 1 hour, cooled to 0°C, and 13.0 g (115 mmol) potassium tert-butoxide were added.

The reaction was stirred overnight at room temperature, then poured into water and extracted with diethyl ether. The combined organic fractions were dried over magnesium sulfate, filtered, and concentrated by rotary evaporator. The crude product was purified by silica gel flash column using 8:1 to 6:1 hexanes to dichloromethane as eluent. 16.67 g of product were collected for 74.4% yield.

Synthesis of DFS

Scheme 2 – Synthetic pathway to DFS. The starting material is prepared following Steps 1 and 2 in Scheme 1.

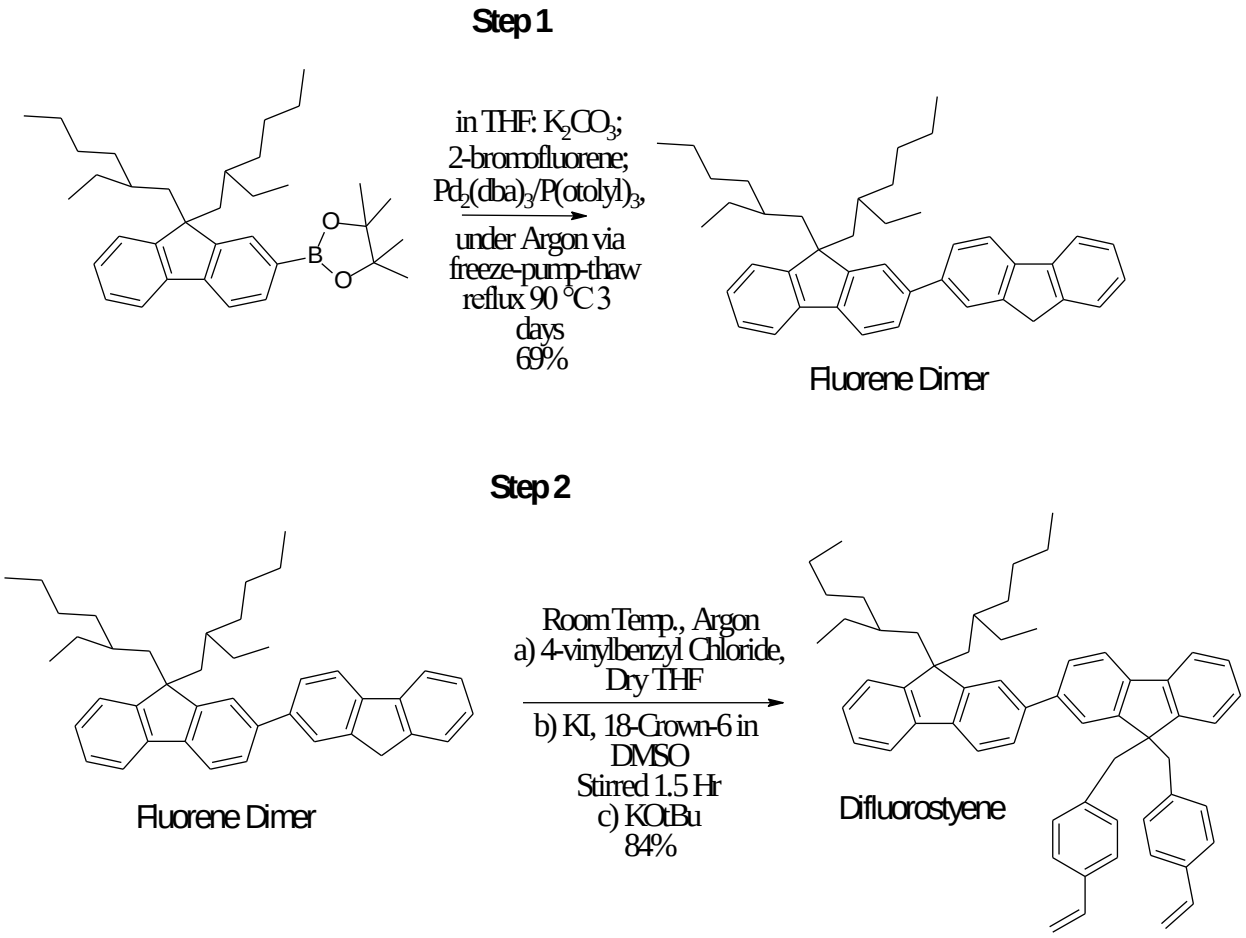

2-{2'-9',9'-bis[(2''-ethylhexyl)-fluorenyl]}-fluorene [Fluorene Dimer]

In a three arm flask, 3.86 g (7.5 mmol) of Int-2 [Scheme 1] and 1.82 g (7.5 mmol) 2-bromofluorene were dissolved in 50 mL tetrahydrofuran. To the solution, 11.2 mL potassium carbonate in 2 M aqueous solution 51.3 mg (0.1 mmol) tri(dibenzylideneacetone)dipalladium(0), and 68.2 g (0.2 mmol) tri(o-tolyl)phosphine were added. The mixture was degassed thoroughly by freeze-pump-thaw, placed under Argon, and refluxed for 3 days at 90°C.

The reaction was removed from heat and extracted with diethyl ether. The collected ether was washed with water and brine. The organic layers were dried over magnesium sulfate, filtered, and concentrated by rotary evaporator to collect a crude product which was purified by flash column, using a 20:1 hexanes to dichloromethane eluent system. A final mass of 2.84 g was recovered for a 69% yield.

2-{2'-9',9'-bis[(2''-ethylhexyl)-fluorenyl]}-9,9-bis(4'-vinylbenzyl)-fluorene [DFS]

In a round bottom flask, 2.84 g (5.12 mmol) of 2-{2'-9',9'-bis[(2''-ethylhexyl)-fluorenyl]}-fluorene was dissolved in 50 mL freshly distilled tetrahydrofuran. The solution was flushed with argon for 15 minutes while cooling to room temperature. A solution of 0.39 g (2.4 mmol) 18-Crown-6 and 0.37 g (1.4 mmol) potassium iodide in roughly 7 mL dimethylsulfoxide was prepared and added to the stirring tetrahydrofuran solution. To the mixture was added 2.50 g (16.4 mmol) 4-vinylbenzyl chloride. The reaction mixture was stirred under argon for 1 hour, cooled to 0°C, and 3.50 g (31.2 mmol) potassium tert-butoxide were added.

The reaction was stirred overnight at room temperature, then poured into water and extracted with diethyl ether. The combined organic fractions were washed with water and brine, dried over magnesium sulfate, filtered, and concentrated by rotary evaporator. The crude product was purified by silica gel flash column using 5:1 hexanes to dichloromethane as an eluent. 3.40 g of product were collected for84% yield.

Synthesis of FBtF

Scheme 3 – Synthesis of FBtF. Synthesis of starting material is shown in Scheme 1.

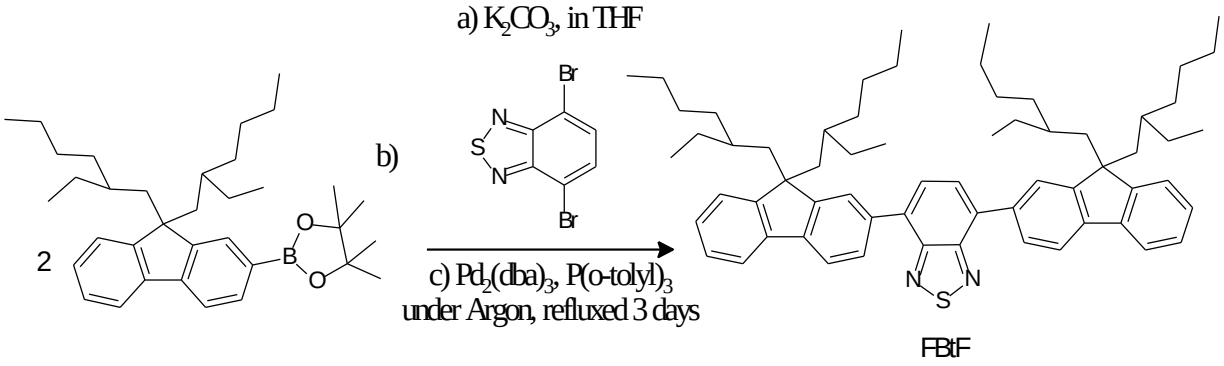

4,7-bis{2'-9',9'-bis[(2''-ethylhexyl)-fluorenyl]}-benzo[c]-1,2,5-thiadiazole [FBtF]

In a 3-arm flask, 1.4 g (4.8 mmol) of 4,7-Dibromobenzo[c]-1,2,5-thiadiazole and 5.41 g (10.6 mmol) of Int-2 [Scheme 1] were dissolved in tetrahydrofuran and stirred under Argon. To the mixture was added 5.6 g of potassium carbonate in a 2M aqueous solution and 0.06 g (0.05 mmol) tetrakis(triphenylphosphine)palladium catalyst. The solution was degassed via freeze-pump-thaw and refluxed for 24 hours. The crude product was extracted with diethyl ether, dried, concentrated by rotary evaporator, and purified by column in a 2:1 hexanes to dichloromethane eluent.

Monolith Fabrication – Vial

General scintillator fabrication was performed based on the following procedural outline. Modifications to specific conditions were required for some compositions. In particular, samples fabricated from mixtures containing ≤ 10 wt.% TFS required an increased curing time. Samples fabricated without initiator also required longer curing times at elevated temperatures.

All samples were cured in shell vials with a nominal internal diameter of 10 mm. Prior to use vials were treated to reduce adhesion between the mold and cured sample. Shell vials were immersed in Piranha Solution for 30 minutes, washed thoroughly with water, and dried in an oven at 130°C for 2.5 hours. Vials were placed in a low vacuum chamber containing a small quantity of (Tridecafluoro-1,1,2,2-tetrahydrooctyl) trichlorosilane for about 1 hour. Vials were removed, washed with hexane, dried, and used.

Solid material – custom monomers and the fluor component – were added to vials under air and the vials were brought into nitrogen atmosphere glove box. VT monomer was degassed by three cycles of freeze-pump-thaw and passed through an Alumina oxide column to remove the 4-*tert*-butylcatechol inhibitor. The purified monomer was added to the vials. Samples were mixed by heating to 70°C to melt TFS[4], vortexing in short bursts of up to one minute, and reheating as necessary to prevent solidification until a uniform, molten solution was obtained. Where indicated, a degassed peroxide initiator, 1,1-Di-(tert-butyl-peroxy)-3,3,5-tri-methylcyclohexane [DTTMC] in a 75% solution in aromatic free mineral spirit was added and samples were vortexed.

Samples were cured for a minimum of 24 hours at the same temperature. Other curing profiles were required for initiator free and low TFS content samples and are described in the Results section. After curing, samples were slow cooled to room temperature and demolded to form plastic cylinders. The cylinder faces were ground to remove menisci and achieve a standard sample size. Course grinding was performed to remove the most material, followed by a finer grit grind to finish sizing and leave a smoother finish. Samples were then polished using a diamond based polishing solution with progressively finer grain sizes from 6 to 3 to 1 μm.

[4] The melting point of TFS is around 65°C.

Monolith Fabrication – Ampule

Under air, components were loaded into ampules with a 10 mm. Samples were degassed via freeze-pump-thaw cycles and ampules were flame sealed under vacuum. Samples were mixed by melting components and vortexing then heated to curing temperatures according to the ramping profile shown in Table 1.

Table 1 – Ramping profile for ampule curing tests.

Step	Ramp Time (hrs)	Final Temperature (°C)	Soak Time (hrs)
1	0.33	75	0.5
2	0.33	115	24
3	0.33	130	48
4	0.33	145	24
5	2	115	24
6	4	75	14

Results

Initial material synthesis achieved only about a 50% yield in each step of the TFS synthesis which was not ideal for easy production at scale. However, improvements to the synthetic and purification methods have led to the high yields described in Scheme 1. Here the four reactions used to produce TFS proceed with a minimum yield of 74% occurring in the final step. The improved process has enabled us to generate quantities of TFS on a 10-20 g scale in good purity for device fabrication. For a reaction yielding 10 g of product, that improvement represents about 2.5 g of product or roughly 14 standard sized scintillator samples. One source of

the increased yield is attributed to better pump performance in the freeze-pump-thaw process in degassing the Suzuki Coupling mixture [Scheme 1, Step 4]. The DFS synthetic pathway mirrors that of TFS and was also successfully completed in high yields.

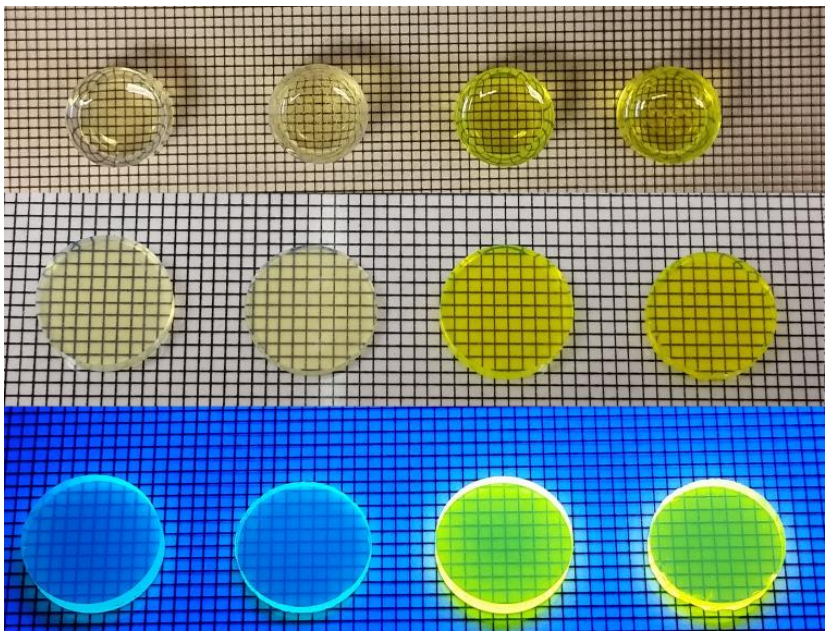

Figure 12 - Examples of fabricated samples using 60 wt% TFS. From top to bottom: as demolded; after polishing; under UV illumination.

With synthesis perfected, the absorption, emission, and excitation of TFS was measured. Peak absorption occurs at 350 nm while the peak emission wavelength of 399 nm is well suited for energy transfer to blue and green fluors. The synthesis of FBtF utilizes the same mechanisms as the TFS synthesis although the synthesis was performed far fewer times given the lower quantity of FBtF required for scintillator fabrication. The photophysics of FBtF were characterized as above, and a peak emission of 520 nm and peak absorption of 420 nm were found.

After synthesis and characterization of the monomer and custom fluor, scintillation samples were prepared. When samples were cured, an increase in TFS content was correlated with decreased required curing time and faster setting of the melt. Quantitative assessment is difficult, but the strongest evidence is a set of samples fabricated to assess the effect of TFS/VT concentration variance. These samples are composed of 1, 5, 10, 20, 30, 40, 50, and 60 wt.% TFS in VT with a minimal amount of initiator to speed polymerization. All samples were

initially cured at 70^{0}C for 26 hours. These conditions are sufficient to completely cure samples with >10 wt% TFS. However the three samples with ≤ 10 wt% were rubbery and required an additional 5 hours at 96 ^{0}C to be completely cured. The increased temperature is in line with conditions needed for samples cured without initiator, although for a much reduced curing time. Based on these trials, the TFS is a more reactive species which promotes rapid polymerization and improves sample setting through cross linking. This also suggests a rational for difficulty in fabricating transparent monoliths from TFS concentrations > 60 wt%. The high reactivity combined with high TFS concentration may lead to poor mixing as samples begin to set during the melt phase and may lead to phase segregation if TFS is selectively more reactive with itself vs VT.

Scintillator robustness is obviously an important quality for a widely utilized detector. Our samples show excellent mechanical qualities after curing. They are solid plastic which polishes well without cracking. Unlike inorganic crystalline scintillators, they are impervious to water and handling in atmosphere. The fluors utilized impart a yellow character to samples, but they are transparent. Though the mechanical properties have not been tested quantitatively, we expect the cross linking character to lead to an improved tensile strength compared to commercial uncrosslinked PVT scintillators.

The ampule curing conditions explored were developed from literature. Very early scintillator work has suggested that unreacted monomer remaining in PVT or polystyrene [PS] scintillators can be a source of quenching[32]. Although we view the lower temperature, shorter term, ambient pressure curing described here as beneficial economically and for the incorporation of potentially labile components, we acknowledge that some higher temperature

curing or post-curing may improve light yield by reducing the concentration of unreacted monomer. To this end, the patent literature regarding scintillator fabrication processes was explored.

The work is spread across PVT and PS, but the general trend has been long curing times broken down into cycles of high and low temperature, with slow cooling over days used to prevent stress developing in monoliths[58–63]. The highest temperatures utilized are universally in excess of those used here – frequently as high as 175°C. Often curing at small sizes is accomplished under vacuum in sealed ampules. We have explored adapting these standards to our needs through the use of ampule curing and the design and testing of a computer controlled heating process. Incorporating the most complex heating cycles, spanning weeks, in our process is impractical. However, a cycle was developed which made use ramping to higher temperature for the benefit of reducing unreacted monomer content as well as ramping back down slowly at the process end to reduce stress on monoliths.

When using pure VT, these curing cycles effectively generate mechanically robust, highly transparent plastic boules. However, addition of TFS to the system causes bubbling and adverse curing – including poor uniformity and transparency. The same tests performed with vinyl toluene mixed with divinyl benzene show identical response. These results suggest that cross linked monomers are not conducive to this curing process. The higher reactivity of TFS versus vinyl toluene may be the cause of these problematic effects at higher temperature where the effect is exaggerated and causes segregation.

Conclusions

The synthetic and fabrication aspects of this project are achieving desired goals. Further modifications to the curing process may improve light yield characteristics at the margins. In particular, a longer time at a lower temperature might begin the curing process slower and reduce the divergence in reaction rate between TFS and VT. Alternatively, the curing process may be more effective under a nitrogen atmosphere even using the more complex cycles suggested by the literature.

III. Scintillator Characterization and Light Yield Measurement

Background

Scintillator samples were characterized in terms of their photoluminescence spectra, light yield, and decay time. Early testing was performed using a CCD camera mounted in a dark box to observe scintillation counts. The setup suffered from poor repeatability in testing geometry, with the sample/source/detector placements being variable. In addition, without

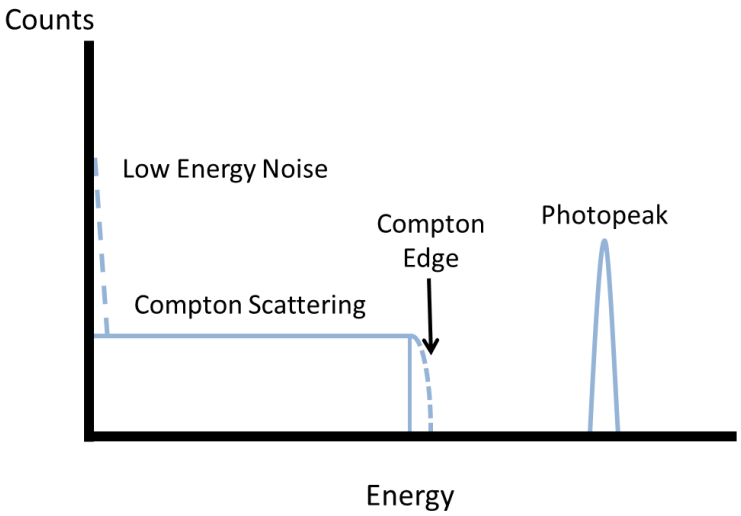

Figure 13 - Idealized representation of a scintillation light yield spectrum, showing the photopeak and Compton Edge. In practice the Compton Edge is usually less well defined. Dashed lines show aspets of non-ideality, for example the broadened compton edge, which result from electronics and photon collection.

shielding of some type, both β- and γ-rays are incident on the sample. The higher stopping power for plastics of β-rays means small differences in sample thickness can have a large effect on the quantity of energy deposited in the material. Finally, the magnitude of response to β-rays is of less interest compared to γ-ray light yield. To combat these issues, the method was discontinued in favor of a more standard PMT based counting approach, described in detail below.

Assessing the performance of novel scintillator materials requires an analysis of their light yield. The light yield is reported absolutely in ph/MeV, however practically measuring this quantity is difficult. In particular, plastics lack a photopeak against which to reference the energy spectra, which is measured as counts within an arbitrarily defined energy bin. Therefore practical measurement of light yield is simplest to do by comparing repeatably identifiable points on the spectrum of a test material against a standard measured and analyzed under the same conditions. The usual point of comparison is the Compton Edge of an energy histogram [Figure 13]. The Compton Edge is the highest energy deposited by a γ–ray interacting via the Compton scattering process – it represents a scattering angle of 180° [Equation 5].

Equation 5

$$\Delta\lambda = \frac{h}{m_0 c}(1 - \cos(\theta))$$

In real spectra the Compton Edge is not a distinct cutoff but a Gaussian edge due to the statistical processes occurring within the PMT during detection and generating current/voltage signals.

An alternative light measurement system was employed to assess the performance of our materials with solid state detectors. These detectors, primarily Silicon Photomultipliers (SiPMs) are small arrays of avalanche photodiodes operated in Geiger mode. They offer a variety of advantages over traditional PMTs including being cheaper, more robust, impervious to magnetic fields, and operating at a lower voltage.[64] The greatest drawback is their comparatively low active area, which can be overcome by tiling SiPMs into larger arrays.

Current SiPM technology has shifted peak photon detection efficiency [PDE] towards lower wavelengths traditionally associated with the blue emission of scintillating crystals. However the optimal PDE of earlier generation SiPMs, such as the SensL M-series MicroFM-SMA-60035 utilized here, occurs at longer wavelengths and is better tuned to a green scintillator such as Eljen's EJ-260 standard. Our samples were compared to the EJ-260 (with a 490 nm emission maximum) due to its better spectral matching to the MicroFM-SMA-60035. Despite the shift to shorter wavelength peak PDE in newer technology, these detectors maintain higher green sensitivity than PMTs and the TFS/FBtF scintillator system described in this manuscript offers a method to make use of this higher wavelength sensitivity.

Experimental

All monolith photo- and radioluminescence characterization was performed after sample preparation, including polishing, was complete. The order of characterization varied.

Photoluminescence Characterization

Photoluminescence spectra were acquired using a Photon Technologies International Quanta Master 4/SE with a xenon arc lamp. To model the light as seen by the PMT for a sample under irradiation, spectra were acquired with the excitation source and emission sensor at right angles. The sample was positioned with an x-θ stage to exclude surface modes. We term this 'semi-transmission' mode.

True transmission mode measurements of monolith emission spectra were performed with monoliths held in a lens holder within an optical cage. This setup was held on a customizable optical breadboard inside of radioluminescence testing dark box. The front face of the monolith was illuminated from one side of the cage by a fiber optic cable connected to an appropriate adapter. Depending on the sample requirements, a ThorLabs Fiber-Coupled LED with an emission wavelength of either 300 or 365 nm was used as a light source. The light source was powered with a Keithley 2200-60-2 DC Power Supply. The opposite side of the cage was coupled to the fiber optic cable intended to pick up sample emission. This cable was connected into an OceanOptics USB2000 spectrometer which fed the collected data to a computer for processing.

Light Yield (Radioluminescence) Measurements

Light yield measurements using a photomultiplier tube were performed in a system custom built on an optical board inside a dark box. Samples were held in a cylindrical Teflon® sample holder and optical grease is applied to the front face. The Teflon® holder and front face of the sample couple directly to and cover the entire the window of a Hamamatsu R878 PMT.

The back of the sample is covered by a thin Teflon® back reflector pressed firmly onto the sample, which is then exposed to a ^{137}Cs γ-ray emitter. Charge signal from the PMT is fed into a Canberra Model 2007P preamplifier then into a Canberra Lynx Multi-Channel Analyzer.

Solid State Detector Radioluminescence Measurements

Solid state detector measurements were taken using a MicroFM-SMA-60035 SiPM and testing board from SensL's M series. The device possesses a 36 mm^2 active area and a 64% fill factor. The peak quantum efficiency of the SiPM is at 500 nm. The sample under measurement was held in a Teflon cylinder [Figure 14]. A back reflector was press fitted against the sample face inside the cylinder, while the exposed face was coupled to the SiPM active area with EJ-550 silicon optical grease. A ^{137}Cs γ-ray emitter was fixed to the sample holder opposite the SiPM. The setup was enclosed in a light tight, grounded metal box.

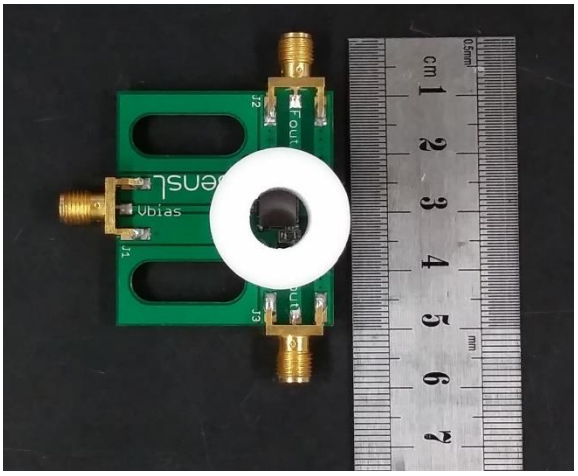

Figure 14 – SiPM with attached sample holder. The sample and back reflector would be inserted into the through hole but are excluded.

Bias was applied to the SiPM with a Keithley 2200-60-2 DC Power Supply. Light pulse signals were amplified with a charge sensitive Canberra 2005 Scintillation Preamplifier to generate a current signal proportional to the number of photons detected. This signal was collected with a PicoScope 5244B oscilloscope and integrated with custom software to obtain an energy value for the pulse. These pulses are then sorted and binned by custom software to build

histograms in the same manner as the multichannel analyzer used to process PMT data. A series of several hundred thousand to in excess of a million data points is measured to develop an Energy vs. Counts plot analogous the PMT data, from which light yield was determined.

Results

After fabrication, the emission spectra of scintillator samples are measured. Emission profiles were taken in two modes - the transmission and 'semi-transmission' - as discussed above. These modes model the light seen by the PMT better than surface emission, because photons generated must pass through a volume of the scintillator prior to collection at the photocathode. In principle, the light seen by the PMT must pass through the scintillator, since the irradiation is coming from the opposite side. In reality, the low stopping power of the plastic scintillator means an approximately equal probability for excitation and subsequent emission to emanate from any part of the scintillator[5].[65,66] Indeed given the opportunity for scattering and self-absorption we might expect to see more emission from the region closer to the PMT. Even with roughly equal photon generation throughout the scintillator volume, the vast majority of that volume is shielded from the PMT window by the bulk of the scintillator. Consequently, the

[5] For a rough sense, we can calculate that a 2 mm sample of PVT should permit the passage of >99% of the 662 keV γ-rays emitted by ^{137}Cs. The ratio of Attenuation of γ-rays is given by the expression:

$$\frac{I}{I_0} = e^{-\frac{\mu}{\rho}*\rho*t}$$

Where I is the number of γ-rays passing through a medium, I_0 is the number of incident γ-rays, μ/ρ is the mass attenuation coefficient which varies with the γ-ray energy, ρ is the medium density, and t is the medium thickness. Here we use μ/ρ for PVT reported by NIST and assume a 1 g/cm^3 density for the sample in line with PVT and polystyrene. These approximations are supported by (1) only a 4% variation of μ/ρ in this energy range between all aromatic containing polymers (PVT, PS, and PET) reported by NIST and (2) that even with a density of 1.4g/cm^3 in line with PET our >99% transmission conclusion is accurate.

transmission mode spectrum is a better match than a spectrum which incorporates the strong emission from an excitation beam incident on the surface of a sample. Self-absorption will red shift emission as seen by the PMT compared to observed spectra which includes surface emission. The actual spectrum as seen by the PMT is important because PMT quantum efficiency is highly dependent on wavelength of the incident light, especially outside the center of its response curve.

After emission measurements, the light yield of samples under irradiation was characterized. Light yield measurements using a photomultiplier tube were performed in a system custom built on an optical board inside a dark box to standardize geometries and radiation dosage. During testing, each sample is coupled to a Hamamatsu R878 PMT using silicon grease and exposed to a ^{137}Cs γ-ray emitter. The Teflon® sample holder surrounds the sample on all other sides, ensuring maximum light collection by reflecting light back into the PMT and shielding the sample from some of the concomitant β-ray irradiation which can generate undesirable low energy signal and does not add to the γ-ray radioluminescence which is the primary metric of interest.

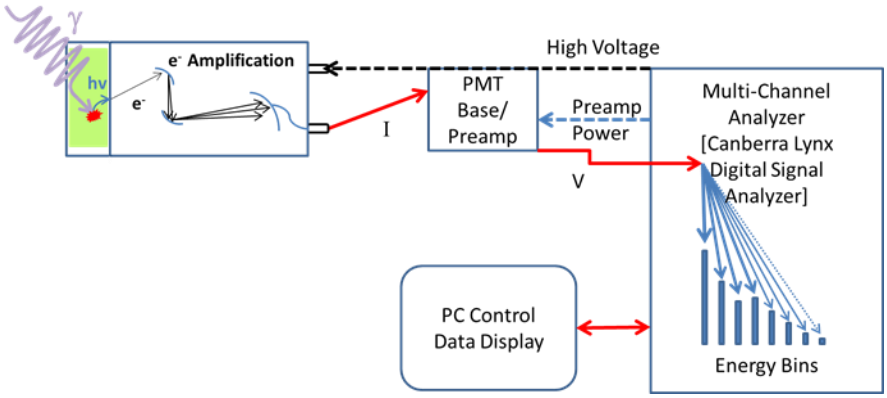

Figure 15 – Schematic of signal processing for light yield measurement system.

When a scintillation event occurs, light is collected by the PMT and the resulting charge signal is fed into a preamplifier. The preamplifier amplifies the current signal and converts it to a voltage, which is processed by a Canberra Lynx Multi-Channel Analyzer. The analyzer bins these voltages to develop a spectrum similar to that seen in Figure 13. A schematic of the signal processing is provided in Figure 15. The Compton Edge is compared to that of an EJ-212 polystyrene commercial scintillator standard which is machined to match the size of the respective sample. In trials, the system shows excellent repeatability. To account for changes in conditions and decaying source strength[6], each set of samples is referenced to a standard measured in the same time span. To confirm the quality of the light yield spectra taken in this system, a baseline test with NaI(Tl) was performed and the results are in line with literature results [Figure 16].[67]

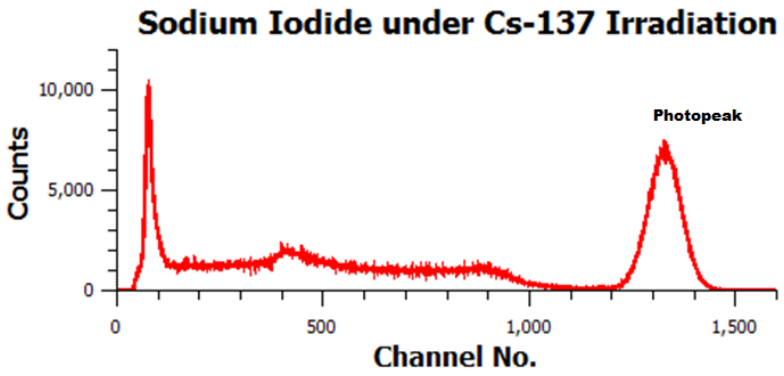

Figure 16 - Spectrum taken in our instrument of NaI(Tl) as a benchmark. The spectrum is a match to literature data. Note the strong photopeak and clear Compton Edge.

The earlier discussion of the effect of TFS concentration on curing was based on a series of samples [Table 2] initially fabricated to assess the effect of TFS concentration on light yield and demonstrate the utility of the compound for scintillator matrices. Inferences about the optimal TFS/VT mixture can be drawn from the samples ranging from 1 to 60 wt.% TFS however it should be noted that none of these samples contain fluor. As noted earlier, samples with a TFS content > 60 wt% are difficult to cure into transparent monoliths.

[6] In practice, source strength decay should be minimal in our time frame – the half-life of Cs-137 is 30 years.

Table 2 – Curing conditions and resulting light yields for TFS/VT samples made without fluor. Samples made with 0.5 wt% initiator. Remaining content is vinyl toluene.

TFS (wt%)	Curing Cycle		Light Yield, %EJ-212, Adjusted
	Hours at 70°C	Hours at 96°C	
1	26	5	76
5	26	5	85
10	26	5	74
20	26	0	70
30	26	0	64
40	26	0	68
50	26	0	60
60	26	0	51

In Figure 17, the raw light yield initially rises with the increase from 1 to 5 wt% TFS, then falls again. The two other data sets on the plot are a consequence of the necessity to correct our light yields to account for the changes in PMT sensitivity with changing wavelength – in particular a much lower quantum efficiency at greener wavelengths [Figure 18]. To

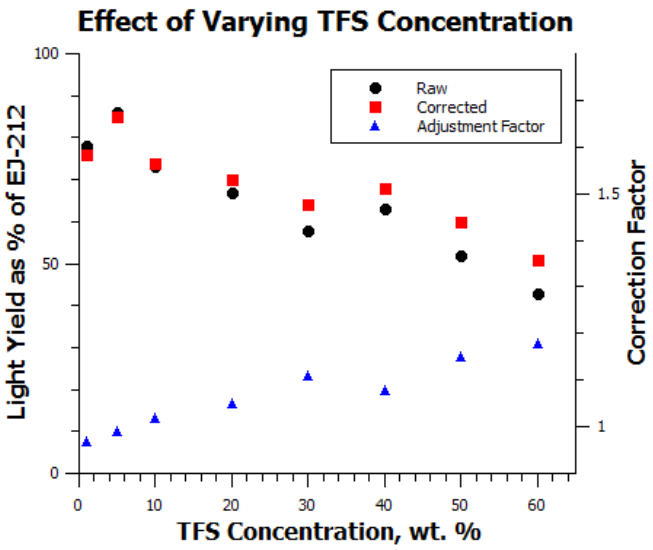

Figure 17 – Plot of the light yield data and associated correction factor for a range of scintillator samples fabricated from a series of TFS/VT compositions. No fluor was utilized in these samples.

address this, we weight the quantum efficiency of the PMT response to each scintillator by its emission profile to create an assessment of scintillator performance on an absolute scale:

Equation 6

$$\bar{Q}_i = \frac{\sum_w Q_{PMT}\,(w)\; x\; I_i(w)}{\sum_w I_i(w)}$$

Where $\overline{Q}_i$ is the weighted efficiency of sample *i*, $Q_{PMT}(w)$ is the quantum efficiency of the PMT at a wavelength w, and $I_i(w)$ is the intensity a sample's emission at wavelength w. Now we can calculate the adjustment factor for a sample i, F_i, in Equation 7:

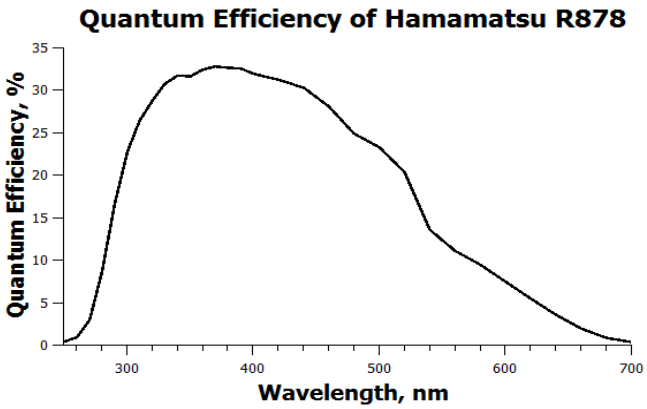

Figure 18 - Hamamatsu R878 Quantum Efficiency.

Equation 7

$$F_i = \frac{\overline{Q}_{standard}}{\overline{Q}_i}$$

The corrected light yield is then simply the raw light yield times the correction factor for a given sample – which generally ranges from 0.9 for samples bluer than the standard up to as much as 2.2 for very green samples.

Now if we reexamine the data above, we can see that the corrected light yield follows the same trend as the raw light yield, while the adjustment factor is steadily rising. This means that while sample emission is becoming greener (driven by the changing composition of the samples), it is not the driving force for light yield reductions. If emission color were the only factor, the correction factor would counteract the trend. The initial rise in light yield is driven by improved scintillation from the incorporation of TFS in the matrix; and the following fall off in performance is driven by self-absorption as increasing TFS is incorporated.

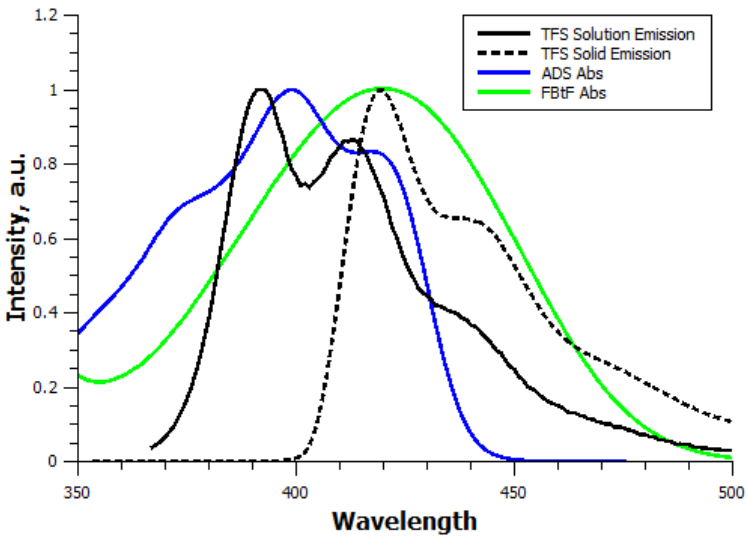

Figure 19 - The emission profiles of TFS (solid and solution) overlaid with the absorption bands of potential fluors.

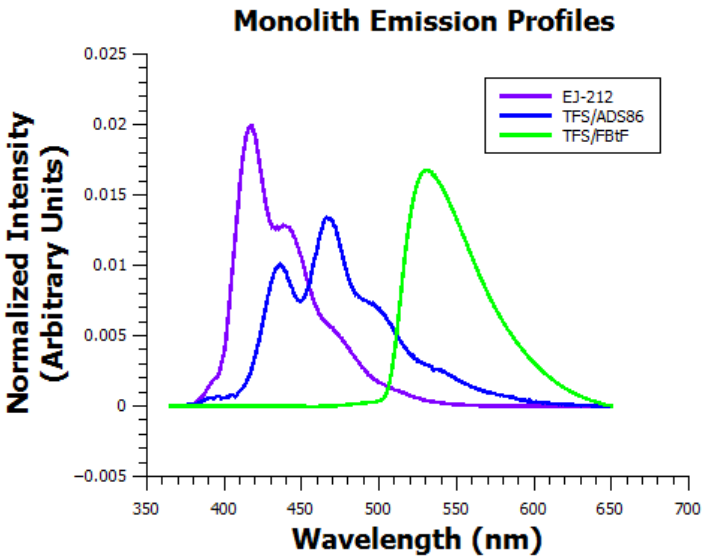

Figure 20 - Emission spectra for TFS/VT samples containing alternate fluors. EJ-212 shown for comparison. Spectra have been normalized to have equal area.

This self-absorption leads to absorption/re-emission efficiency losses in addition to observed red-shifting.

The two extremes of this unshifted sample series are chosen for further exploration via incorporated wavelength shifters. At the high light yield/low TFS content extreme, wavelength shifter is added to the 5 wt% TFS sample to demonstrate that these samples cannot be significantly improved with this change - indicating TFS is not suitable as a primary dye. Wavelength shifter is also incorporated in the low light yield/high TFS content (60 wt%) samples to demonstrate that the matrix can achieve a high light yield with reduced self-absorption.

The two dyes utilized in these samples were a commercially available fluor candidate, ADS086BE [ADS86] from American Dye Source and the synthesized fluorene-based compound FBtF. FBtF has a much greener emission spectrum than an ideal candidate. After exploring commercially available candidates (generally OLED materials) for possible selections, the compound ADS086BE [ADS86] from American Dye Source was chosen. The emission spectrum is a closer match to the desirable blue range, while still absorbing in the range of TFS emission – with peak absorption of 397 nm.

The primary features of a fluor are strong energy transfer from the matrix and solubility. The energy transfer is assessed through the respective absorption/emission spectra and the emission profile of mixtures containing both compounds. Above a required fluor concentration, these mixes demonstrate only fluor emission and show minimal to no emission in the TFS region. The combination indicates a strong tendency for excitation to transfer to the fluors prior to emission. When considering the suitability of a fluor in terms of its solubility, in general the loading is low enough that only moderate solubility is required. For the two fluors described, the main drawback for FBtF is a peak emission of about 550 nm – meaning scintillators based on this system are green emitting and not ideal for common, blue sensitive PMTs [Figure 20].

For our initial testing of 5 wt% TFS in VT with a wavelength shifter, ADS86 was chosen and a series of samples was prepared at that concentration with a range of ADS86 from 0.2% to 1%. The results show no major improvement over the standard, with a light yield of roughly 102% versus the commercial standard for most compositions. Therefore with an appropriate wavelength shifter, the formulation utilizing TFS as primary dye type concentration (albeit at a higher, 5 wt% loading than generally used for this purpose) does not achieve markedly improved light yields.

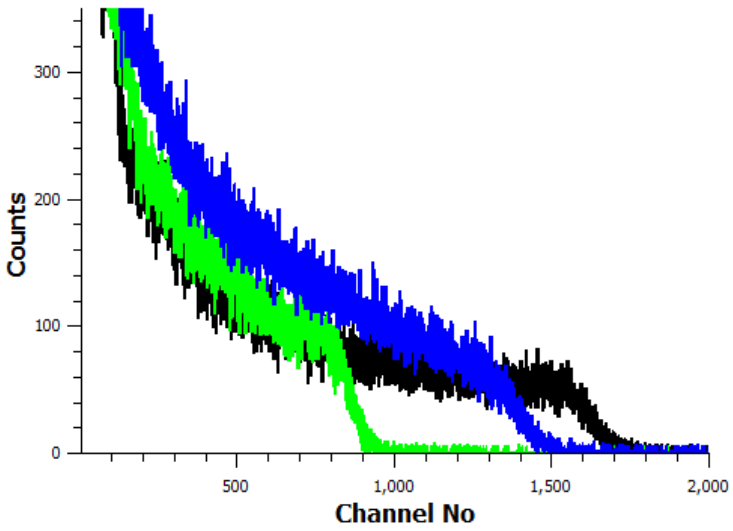

Figure 21 - Light yield data measured by PMT for top performing TFS/VT samples with ADS86 (blue) and FBtF (green). EJ-212 shown for reference (black).

For fabricating the high TFS content samples, an analysis of optimal primary dye concentrations is required. The initial results with the TFS/VT/FBtF system show that lower fluor concentrations, in the 1.5 wt.% range generate better results. As a result these levels are employed to show that using the 60/40 TFS/VT system can significantly improve on standard light yield. These samples show a 27% improvement in light yield over EJ-212 using FBtF as a dye and 23% using ADS86.

Additionally, samples fabricated without initiator generally show slight improvement over those cured with DTTMC. This is not unexpected based on early scintillator literature[32]. The tradeoff is that curing requires a longer time and higher temperature. However, overall light

yields achieved with these samples are significantly lower than those shown by the commercial standard [Figure 21].

Alternative Matrix Materials

Scintillators using DFS were prepared from a mixture of DFS and VT with BBOT as a primary dye. Although a loading of up to 70 wt% DFS in VT could be achieved in these samples and the energy transfer from DFS to BBOT is expected to be efficient based on their spectral overlap [Figure 22], the ultimate results were not promising. In the end, these systems received substantially less attention because even top performing samples achieved adjusted light yields of only 80% of EJ-212. Improvement of DFS performance may necessitate the use of a fluor with higher quantum efficiency. The BBOT utilized possesses a quantum efficiency of 74%.[68] However even a high efficiency fluor is not expected to reach significant improvements over the TFS system. Therefore, research focus was primarily on TFS and its higher performance, and attempts to improve this performance through the use of alternative curing methods, followed by our work in triplet harvesting explored later.

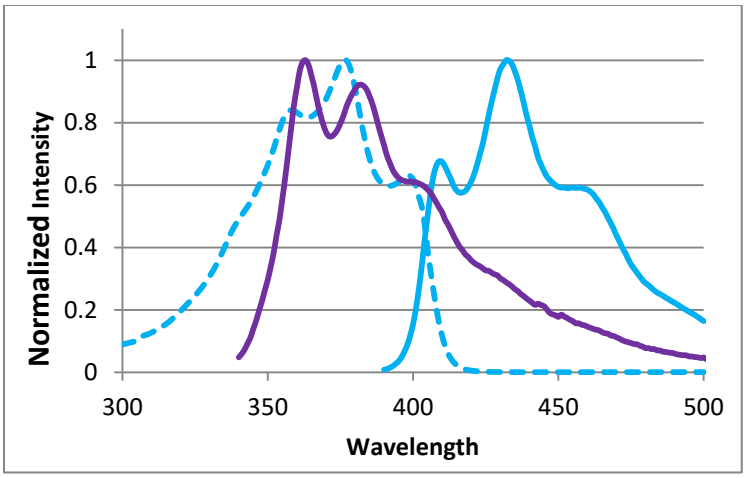

Figure 22 – The spectral overlap between DFS emission (purple) and BBOT absorption (dashed blue) is shown. The emission spectrum of BBOT (solid blue) is also shown.

Solid State Results

As discussed, solid state detectors are of interest for their better sensitivity to higher wavelengths and advantages over PMTs. To assess the performance of our scintillators when using a SiPM, the EJ-212 standard was replaced with EJ-260. This standard is designed for use in applications requiring green emission color – with including light piping and solid state photosensors. The peak emission is 490 nm, making it a more natural comparison for our material under these conditions than EJ-212. Measurements were originally attempted with a single Hamamatsu Avalanche Photodiode, but due to the small photosensitive area and low gain were unsuccessful.

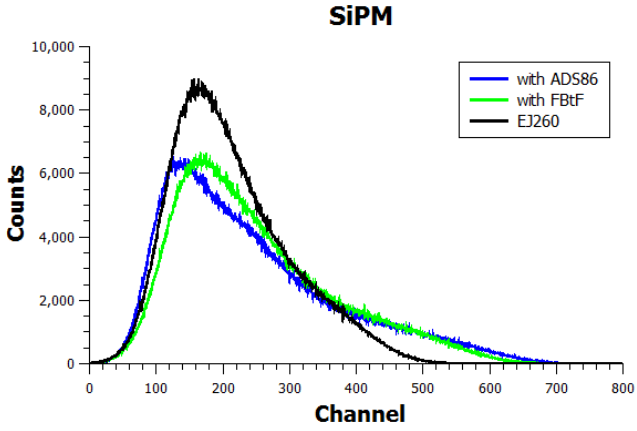

Figure 23 – SiPM data.

The analysis of SiPM data described above generates a Counts vs Channel plot identical in concept to those generated by the multichannel analyzer used to collect PMT data [Figure 23]. Exactly as with PMT light yield determinations, the key feature is the highest energy cutoff. While increased counts contribute to building a smooth spectral curve, they should not affect computation of light yield as long as the counts exceed the minimum to accurately resolve features in the critical region of the spectrum (i.e.: the Compton edge)

Spectra were acquired well above the necessary counts numbers to improve curve quality for this manuscript. The measurement setup makes precisely equalizing these pulses somewhat difficult. In In the PMT data, an extremely strong peak on the far left of the plot represents the lowest energy noise in the data. Here that peak is absent, presumably due to a higher threshold for detection in the SiPM. This has the practical effect that fewer counts are acquired for a given time period. Analysis of the data [Figure 23], shows that the light yield of the top performing TFS/VT samples containing FBtF and ADS86 fluor exceed the light yield of the EJ-260 green standard by 25% and 31% respectively. This demonstrates the clear utility of our samples for green detector applications, including pairing with light guides which are better suited for green emitting scintillators.

Conclusions

Of the matrix materials synthesized and characterized, the performance of the TFS/VT system is our most promising result. It represents an improvement over standard, commercial scintillator formulations in ph/MeV – showing a 27% maximum improvement. This translates to a 12,700 ph/MeV light yield. The success of this system using high concentrations of TFS and

incorporating fluorene moiety containing fluors shows the utility of OLED materials in general and fluorenyl materials in particular for improving plastic scintillator technology.

Further, the success of the system when used with SiPMs and the substantial outperformance of the green standard technology opens up a new range of uses for the materials studied. These applications include pairing with new types of detectors, making use of the higher green sensitivities available in solid state detectors, and better compatibility with light pipping required in certain contexts.

In addition to the overall promising performance of the scintillators herein, the substantial synthetic yields and easy fabrication of samples shows a proof of concept of the new classes of materials employed. The synthetic pathways demonstrate a high yield and the potential to engineer materials specifically for scintillation purposes with low melting temperature and curability.

IV. Triplet Harvesting Approaches to Increased Light Yield

Background

Improving scintillator light yield requires expanding the energy available to the scintillator to produce photons. Sections II and III have dealt with increasing the efficiency of converting excitation to light through improvements in scintillator materials and formulation. This section focuses on increasing the available pool of excited states for photon production. As previously discussed, excitons created in the scintillating medium are statistically produced in a ratio of 3:1 triplet to singlet state. Traditional scintillators harvest singlet states through fluorescent fluors. By incorporating phosphorescent or TADF dopants with triplet states

energetically favorable for transfer from the triplet state of the matrix, we aim to access a significant portion of this other 75% of the energy deposited in the medium.

Iridium complexes are frequently used for a similar purpose in OLED devices.[69–73] These complexes overcome the spin-forbidden transitions through spin-orbit coupling, which increases the singlet character of the triplet state and increases the efficiency of intersystem crossing. The rate of radiative ^{1}T-^{0}S transitions is increased generating more photons. It should also be noted that this changed character of the triplet state increases the efficiency hoping between singlet and triplet excited states – potentially allowing collection by phosphorescent dopants of singlet excitons in the matrix or transfer of triplet excitons to a secondary fluorescent fluor with high quantum efficiency.[74] With the goal of achieving higher light yield from these materials, the well-known Iridium complex bis[2-(4,6-difluorophenyl)pyridinato-C2,N](picolinato)iridium(III) [commonly abbreviated FIrPic, Figure 24] was explored as a candidate complex.

Both organometallic complexes and TADF compounds require modifications to improve solubility without affecting the photophysical properties. For the reasons described in Section I, both these materials require high loading in the polymer melt to achieve the desired effect. As with fluorene, Iridium complexes, in particular FIrPic, are popular in OLEDs for the same properties that make them interesting in scintillator work. As a result, a wide variety of work has examined use of Iridium complexes in polymeric material. In a comprehensive review[75], Ulbricht et al. describe five methods of curing the metal complexes into the polymer itself – i) decoration of (co)polymers with complexes; ii)

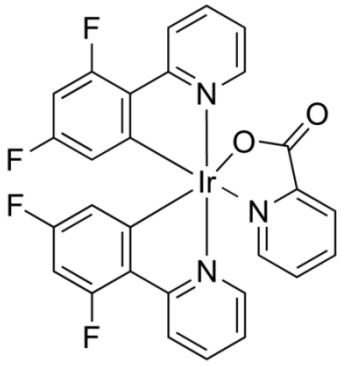

Figure 24 – Structure of FIrPic.

complexation at (co)polymers; iii) (co)polymerization by complexation; iv) complex as (co)polymerization initiator; and v) (co)polymerizing complex monomers. Although organometallic complexes tethered to curable moieties were considered to reduce aggregation issues with organometallics in high loadings, synthetic difficulties were encountered and alternative approaches to triplet harvesting were sought. A candidate complex is shown in Figure 25. Incorporation of long aliphatic chains were preferred for their ability to increase the miscibility of compounds in the hydrocarbon, non-polar matrix matrix without adding labile or potentially photo-active functional groups which could lead to unintended consequences.

The large scale use of organometallic complexes carries with it a dependence on an expensive and rare resource – generally Platinum or Iridium. OLED devices have sought to avoid this issue by the use of other materials employing alternative strategies such as triplet-triplet annihilation, hybridized local and charger transfer, and thermally activated delayed fluorescence [TADF] to expand the available energy for radiative decay.[76–81] Certain organocopper complexes have been shown exhibit TADF, however it is the organic TADF compounds are of primary interest here.[82] In contrast to the organometallic dopants, which achieve radiative ^{1}T-^{0}S transitions through strong spin/orbital coupling, TADF materials do not radiate directly from the triplet state. Instead their role in triplet harvesting is to allow thermally assisted hoping of excitons from the T^1 level to the S^1 level through reverse intersystem crossing

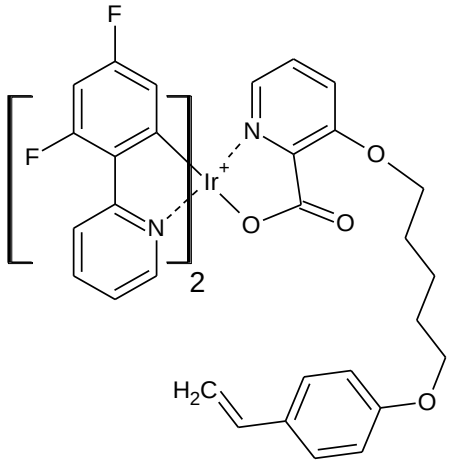

Figure 25 – Structure of IrHS

(RISC). The T_1 state is always lower energetically than the S_1 state, making RISC is an endothermic process. However given a small enough ΔE_{ST}, RISC will occur through utilization of the available thermal energy of the system. The endothermic promotion thus achieved yields singlet excited states which are capable of generating delayed fluorescence due to their non-spin-forbidden transition to the ground state. Consequently, the 25% statistical limit in fluorescent materials can be exceeded to achieve up to 100% in non-metallic organic molecules. In addition the all organic nature of TADF materials is seen as a benefit in the scintillator application in terms of solubility in the polymer melt.

Literature compounds were explored for TADF candidate compounds. Two compounds were initially chosen and synthetic schemes were designed to incorporate solubility promoting hexyl and octyl chains into the materials. As seen in Figure 26, the compounds were a dual m-dicyanobenzene core with carbazole side groups (TADF1) and a core of 9,9-dimethyl-9H-thioxanthene 10,10-dioxide with acridine side groups (TADF2).[83,84]

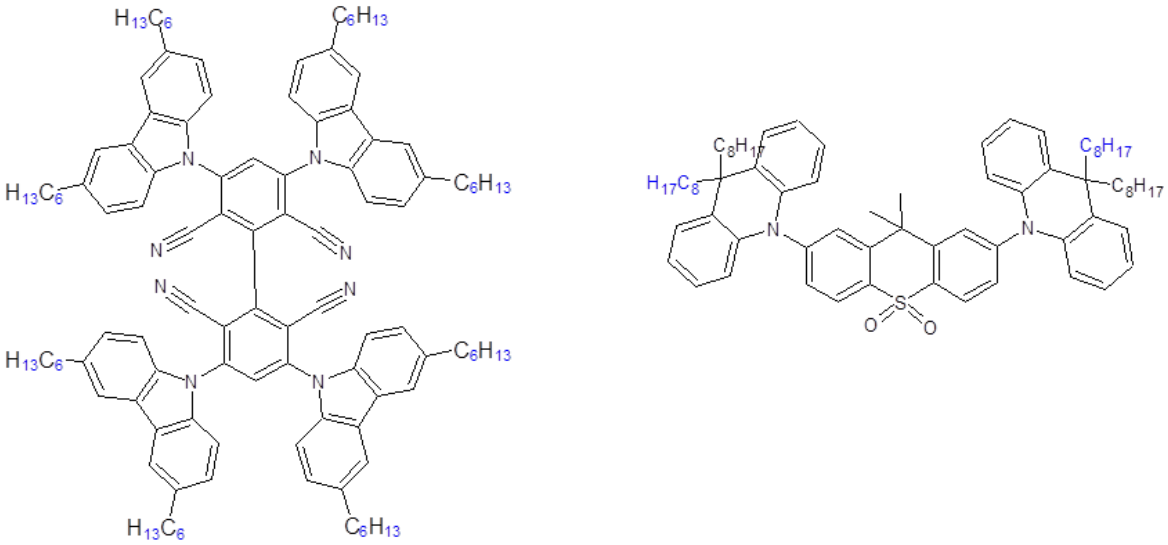

Figure 26 - Examples of TADF compounds of interest. These are theoretical solubility improved versions of literature compounds.[83,84] TDAF1 (left) and TADF2 (right) were never successfully synthesized.

In both instances, synthetic work stalled either due to inability to produce literature procedures (in TADF1) or difficulties arising from the effect of structural modifications on the synthetic pathway (in TADF2). As a result, the side groups of TADF1 were combined with the core of TADF2 to create a new material 2,7-bis(N-3',6'-dihexylcarbazole)-9,9-dimethyl-9H-thioxanthene-10,10-dioxide, known as DMT-DCz [Scheme 6].

DMT-DCz was characterized photophysically to determine its suitability for scintillator use and its solubility in PVT and poly(vinly carbazole) [PVK] matrices was explored. At the high loadings sought for triplet harvesting, miscibility with the matrix is critical to achieving performance improvements. These high loadings cause the same self-absorption issues as the TFS matrix experiences and so a wavelength shifter is a necessity. By matching absorption spectra from the catalog of fluorescent compounds on hand to the emission spectrum of DMT-DCz, a wavelength shifter is was selected. Samples were prepared and characterized.

Experimental

General procedures were followed similar to those described above. All solvents used were ACS grade. Where used, dry tetrahydrofuran was freshly distilled over sodium benzophenone. Water work ups were performed with deionized water. Structures were verified by proton NMR using a Bruker AV 400. Photophysical characterization of prepared and commercial compounds in solution was done using a Photon Technologies International Quanta Master 4/SE with a Xenon arc lamp and a Shimadzu UV-1700 PharamSpec UV-VIS spectrometer. Monoliths were polished to the desired size as described in Chapter II. Monolith

characterization of both photoluminescence and radioluminescence (using a PMT) was performed as described in Chapter III.

Synthesis of DMT-DCz

Scheme 4 - Carbazole synthesis portion of DMT-DCz.

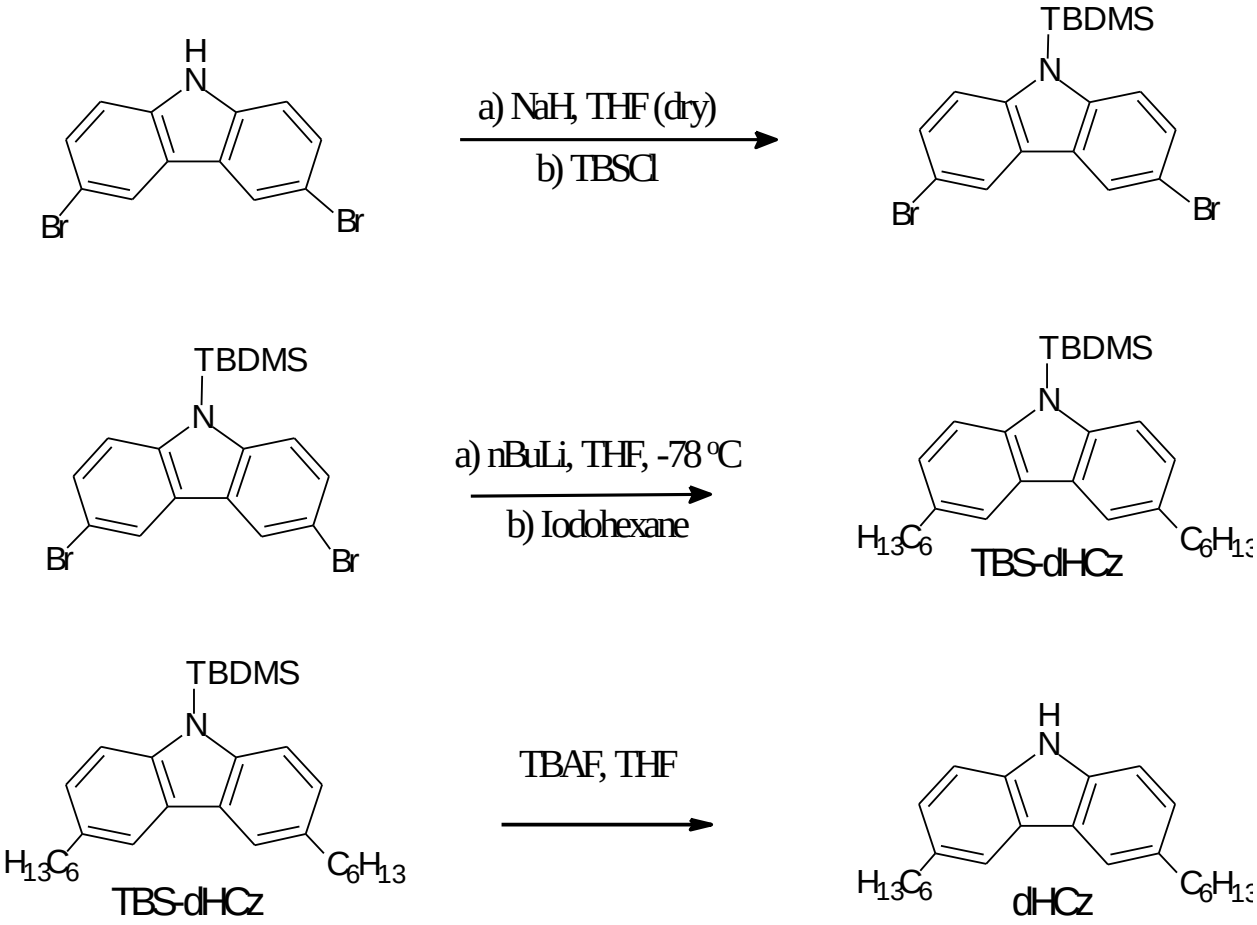

Scheme 5 - Core synthesis portion of DMT-DCz.

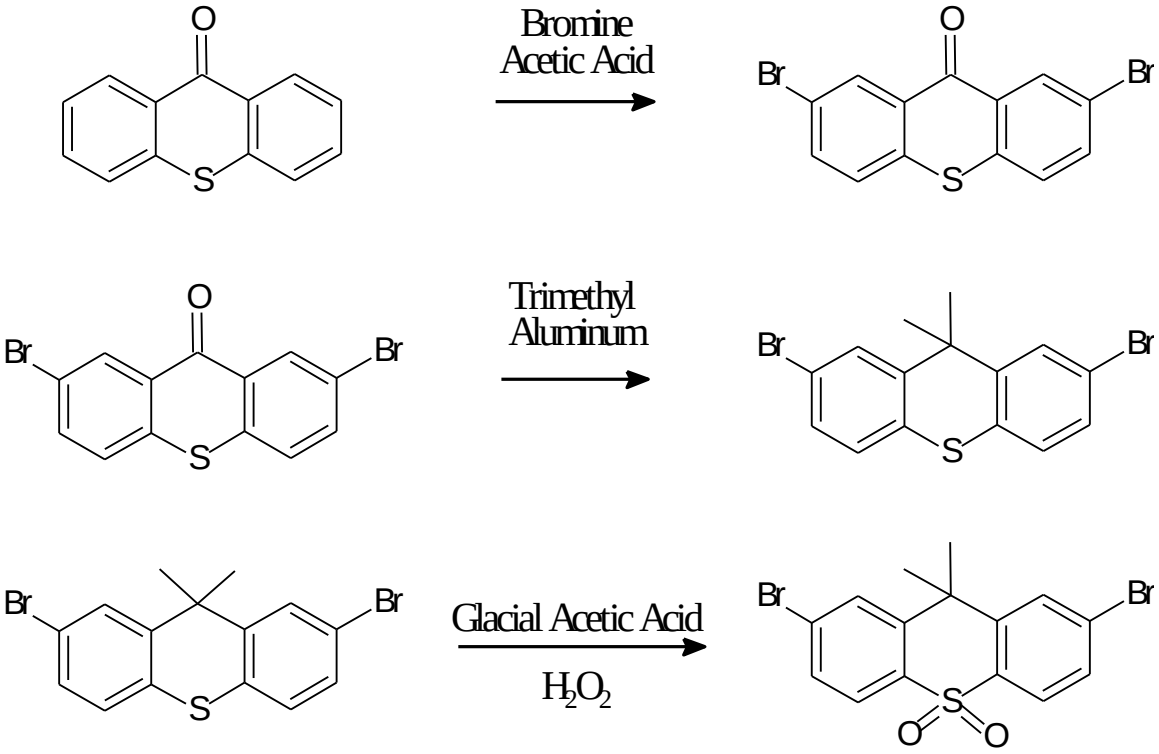

Scheme 6 - Coupling portion of DMT-DCz synthesis.

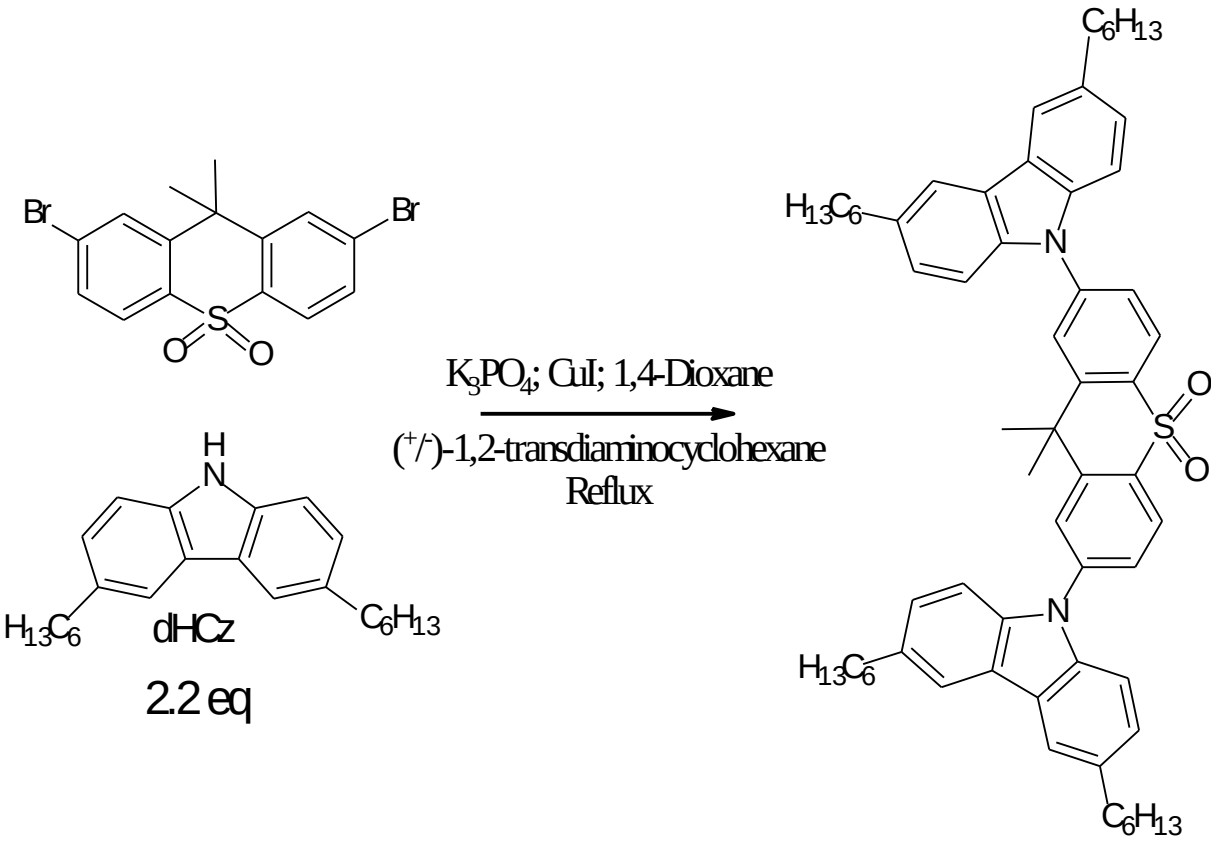

2,7-Dibromo-9H-thioxanthen-9-one

To a solution of 2.5 g (11.8 mmol) 9-H-Thioxan-9-one in 50 mL acetic acid, 5 mL (97.6 mmol) Bromine were added dropwise over 12 minutes. The solution was refluxed for 20 hours in air then cooled to room temperature. A yellow solid was filtered out and washed with methanol. The crude product was dissolved in 400 mL of boiling toluene, recrystallized, and filtered; then recrystallized again in 150 mL Toluene. The product was collected and dried to yield 1.86 g (43% yield).

2,7-Dibromo-9,9-dimethyl-9H-thioxanthene

Under Argon, 1.86 g (5.0 mmol) of 2,7-Dibromo-9H-thioxanthen-9-one was dissolved in thoroughly dry, degassed Toluene. The solution was cooled to 0 °C in an ice bath and 5.6 mL (11.1 mmol) of Trimethyl Aluminum 2M in Toluene was added slowly. The reaction was stirred for 4 hours at 0 °C then at room temperature overnight, after which the reaction mixture goes from a slurry to a clear brown solution. The reaction was poured into ice water and HCl and extracted with dichloromethane. The organic layer was washed with water, then dried over $MgSO_4$ and concentrated on rotary evaporator. The crude product was purified on SiO_2 gel in hexanes to yield 1.81 g of product for a 94% yield.

2,7-Dibromo-9,9-dimethyl-9H-thioxanthene-10,10-dioxide

In a 250 mL round bottom flask, 1.81 g (4.7 mmol) of 2,7-Dibromo-9,9-dimethyl-9H-thioxanthene were heated at 80 °C in glacial acetic acid. To the mixture were slowly added 12 mL of H_2O_2 and the reaction was refluxed for 2 hours.

The mixture was left to cool to room temperature and 25 mL water were added to precipitate a white solid. The solid was collected via Buchner funnel and placed under high vacuum while heating[7] to remove water. A yield of 1.49 g (76%) was recovered.

[7] In a later attempt to fully dry the product in the vacuum oven, the compound melted at >180°C, be aware of this issue.

9-Tertbutyldimethylsilyl-3,6-dibromocarbazole

In a 500 mL flask, 1.30 g (32.4 mmol) of sodium hydride, 60% in paraffin, was dissolved in 75 mL of dry THF and cooled to 0 ºC. A solution of 8.70 g (27.0 mmol) 3,6-dibromocarbazole in 60 mL dry THF was prepared in an addition funnel and added dropwise to the sodium hydride solution.

The solution was warmed to room temperature and stirred for 30 minutes, then 4.48 g (29.7 mmol) Tetrabutyldimethylsilylchloride was added against a flow of Argon. The reaction was stirred 1 hour and progress was analyzed by TLC in 2:1 hexanes : ethyl acetate to demonstrate completion. The reaction was poured into 250 mL H_2O and extracted with 3x175 mL diethylether. The organic layers were washed with 250 mL brine, dried over $MgSO_4$, and filtered to remove the solid. The ether was concentrated on rotary evaporator and dried on a vacuum line to yield 9.60 g crude product.

The crude product was dissolved in dichloromethane, and adsorbed onto 48 g of SiO_2 gel. The silica/crude mixture was purified by flash column using 1 L of dry silica gel with a 20:1 hexanes:dichloromethane eluent system. A final yield of 95% was collected.

9-Tertbutyldimethylsilyl-3,6-dihexylcarbazole

In a 250 mL 3 arm flask, 5 g (10.6 mmol) 9-tertbutyldimethylsilyl-3,6-dibromocarbazole was dissolved in 140 mL dry tetrahydrofuran under Argon. The solution was stirred and cooled to -78ºC and 9.32 mL (23.3 mmol) n-butyllithium 2.5 M in hexanes was added dropwise. The

solution was stirred 1 hour and 6.36 g (26.5 mmol) iodohexane was added. The reaction was allowed to warm to room temperature overnight, then quenched with 10 mL saturated ammonium chloride and poured into 300 mL water. The product was extracted with 3x200 mL diethyl ether. The Organic layers were collected and washed with 300 mL each of saturated sodium sulfate and brine, then dried over magnesium sulfate, filtered, and concentrated by rotary evaporator. The crude product was purified by flash column in hexanes to recover 4.53 g (95% yield).

3,6-dihexyl-9H-carbazole

In tetrahydrofuran, 12 mL (12 mmol) of tertbutylammoniumfluoride 1 M in hexane was added to 4.53 g (10.1 mmol) 9-tertbutyldimethylsilyl-3,6-dihexylcarbazole and the solution was stirred 1.5 hours. The reaction mixture was concentrated on rotary evaporator, then diluted with diethyl ether. The resulting solution was washed with 250 mL of brine and 2 x 250 mL water, then dried over magnesium sulfate, filtered, and concentrated on a rotary evaporator.

The crude product was purified by flash column using an eluent system of 3:1 hexanes : dichloromethane. A white solid product was collected after concentration and drying.

2,7-bis(N-3',6'-dihexylcarbazole)-9,9-dimethyl-9H-thioxanthene-10,10-dioxide

Under nitrogen atmosphere, 0.44 g (2 mmol) of potassium phosphate tribasic was loaded into a schlenk flask. The flask was sealed and removed from the glove box to place on an argon

line. Against an argon flow, 0.20 g (0.47 mmol) of 2,7-Dibromo-9,9-dimethyl-9H-thioxanthene-10,10-dioxide, 0.35 g (1 mmol) of 3,6-dihexyl-9H-carbazole, and 0.01 g (0.05 mmol) copper iodide were added. A reflux condenser was placed under argon by vacuum and refill using a vacuum adapter and female stopper. While flowing argon the reflux condenser and schlenk flask were coupled. To the flask was added 12 mL 1,4 dioxane and the reaction mixture was stirred till reactants were dissolved or dispersed. To the mixture was added 0.02 g (0.2 mmol) of (+/-)-1,2-transdiaminocyclohexane. The reaction mixture was refluxed for 24 hours.

The reaction mixture was cooled to room temperature, poured into mL of water, and extracted with dichloromethane. The combined organic layers were dried over magnesium sulfate, filtered, and concentrated by rotary evaporator. The crude product was purified by silica gel flash column in a hexanes : dichloromethane eluent system ramped sequentially from 4:1 to 1:2. A yield of 0.36 g crude product (82%) was recovered.

Photophysical Measurements

Quantum yield and phosphorescence characterizations of compounds were performed in the Photon Technologies International Quanta Master 4/SE using a Xenon arc lamp and Xenon flash lamp, respectively.

Measurements of the Quantum yield were performed by comparison to a 9,10-diphenyl anthracene [DPA] standard. In six 10 mL volumetric flasks, three solutions each of DMT-DCz and DPA were made at a range of concentrations. Based on prior measurements, the concentrations were selected to give a large range of absorbance values up to 0.1 Abs. All

solutions were degassed via freeze-pump-thaw in Schlenk bombs and aliquots were transferred into screw cap cuvettes in a nitrogen atmosphere glove box. The photoluminescence spectra were acquired using the sealed cuvettes and the appropriate excitation wavelength. Spectra were corrected for the intensity of excitation wavelength generated by the Xenon lamp.

Determination of the triplet state was performed by measuring the phosphorescent emission. A 9.6 μg/mL solution of DMT-DCz was prepared in dry toluene and degassed through freeze-pump-thaw in a Schlenk bomb. The resulting solution was added to a screw top quartz EPR tube under nitrogen atmosphere and sealed. The sealed tube was immersed quickly in liquid nitrogen to freeze the toluene into an optical glass. Measurements were performed over 100 averages for spectral quality using a Xenon flash lamp with a delay in acquisition to exclude fluorescent emission modes.

Monolith Fabrication

All commercial monomers were purified prior to use. In addition, liquid monomers were degassed through freeze-pump-thaw. Vinyl toluene was purified as described in Section II by removal of 4-*tert*-butylcatechol inhibitor. N-vinylcarbazole (NVK) was purified by vacuum sublimation. Methyl methacrylate (MMA) monomers were passed through a column packed with MEHQ inhibitor remover.

<u>Monoliths Containing Iridium Complexes</u>

Iridium complexes were pre-dispersed in TFS by dissolution of both compounds in optical grade chloroform. The solution was then dried to a solid with which was mixed with vinyl toluene in the appropriate ratio under nitrogen atmosphere.

TADF/PVT Monolith Fabrication

Monoliths containing DMTDCz were fabricated, demolded, polished, and measured in accordance with techniques described in earlier chapters. Monoliths were made from pure vinyl toluene matrix and cured for 24 hours at 80 ºC.

To prepare monoliths using wavelength shifters, solutions of the WLS were prepared in optical grade chloroform in 10 mL volumetric flasks at a concentration of roughly 1 mg/mL. Depending on the precise concentration, the appropriate aliquot of solution (~200 µL) was added to a prepared shell vial and the solvent was evaporated with careful application of compressed air.

TADF/PVK/PMMA Monolith Fabrication

The DMT-DCz/PVK/PMMA samples were fabricated via one of two different routes. In Route 1 the NVK and DMT-DCz were added as solids then mixed after melting in the glove box. In Route 2 the NVK and DMT-DCz were dissolved in a minimal amount of spectroscopic grade chloroform along with the wavelength shifter then carefully dried to a solid, creating a mixture prior to melting.

Route 1

Wavelength shifter was added as with the PVT samples, then the solid NVK and DMT-DCz components were added to the shell vial. Samples were brought into the glove box and purified MMA was added. The samples were melted at 65°C and vortexed as necessary to create a homogeneous solution. During vortexing, the sample was returned periodically to the heating block to maintain a liquid phase.

After samples were thoroughly mixed, Luperox® 231 from Sigma-Aldrich was added and the sample was briefly vortexed once more. Samples were then heated to 80°C at a rate of 4°C/hr, then cured at 80°C till 24 hours had elapsed since the beginning of the ramp. After curing was complete samples were allowed to slow cool in the heating block before being removed.

TADF/PVK/PMMA Monolith Fabrication – Route 2

Wavelength shifter in solution was added to solid NVK and DMT-DCz in a shell vial. A minimal amount of spectroscopic grade chloroform was added as necessary to dissolve the components, and the sample was dried back to a solid. Samples were brought into the glove box and purified MMA was added. The samples were melted at 65°C and vortexed as necessary to create a homogeneous solution. During vortexing, the sample was returned periodically to the heating block to maintain a liquid phase.

After samples were thoroughly mixed, Luperox® 231 from Sigma-Aldrich was added and the sample was briefly vortexed once more. Samples were then heated to 80°C at a rate of 4°C/hr, then cured at 80°C till 24 hours had elapsed since the beginning of the ramp. After curing was complete samples were allowed to slow cool in the heating block before being removed.

Results

Iridium Complexes

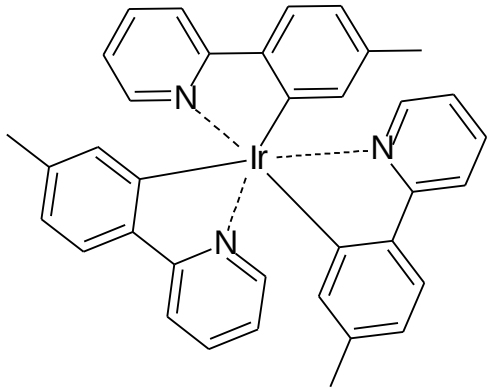

Figure 27 – Structure of $Ir(mppy)_3$.

Analysis of triplet harvesting dopants began with straightforward solubility tests of FIrPic and tris(2-(p-tolyl)pyridine-C2,N') Iridium(III) [known as $Ir(mppy)_3$, Figure]. For making TFS/VT samples with phosphorescent dopants, the Iridium complexes were pre-dispersed in TFS by dissolution of both compounds in optical grade chloroform. The solution was then dried to a solid mixture of TFS and Iridium. The solid was then mixed with vinyl toluene in the appropriate ratio and cured as described above. The premixing of Iridium complexes and TFS solid makes initial dispersal of the phosphorescent compounds achievable. Without this step, dissolution of these complexes is extremely difficult, likely due to the initial tendency of the Iridium complexes to aggregate.

At low concentrations, unsuitable for triplet harvesting, samples containing FIrPic which are fabricated in this manner can be made transparent in solution and when cured. However above 3% we see crystallization of FIrPic despite our pre-dispersal of the fluor in the matrix.

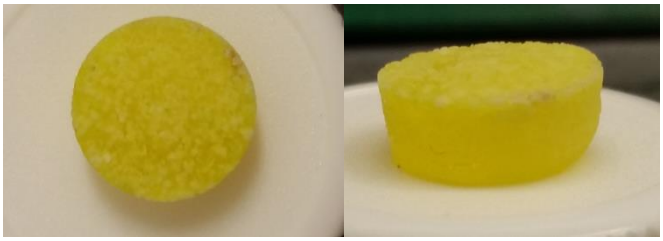

Figure 28 – PVT monolith with 3.8 wt% FIrPic. Crystallization is evident when seen from the top (left) and deformation of sample clear from the side view (right).

The results of the 3.8% FIrPic loading test

can be seen in Figure 28. Dopant aggregation is clearly evident on the top face and the circumference of the sample is highly irregular, indicating a shrinkage during curing.

To counteract this, the functionalization of FIrPic to improve its solubility was explored. First we examine IrEH, a FIrPic complex modified with an ethylhexyl side chain to improve solubility [Figure 29]. Of primary concern is the effect of this alteration in structure on the photophysical properties of the fluor. An examination of the phosphorescent spectrum of IrEH [Figure 30] clearly demonstrates the additional moiety has at most a minimal influence on the desired energy level structure through comparison with literature FIrPic spectra and triplet state measurements.[85] With this assurance, the use of IrEH in scintillator samples was explored.

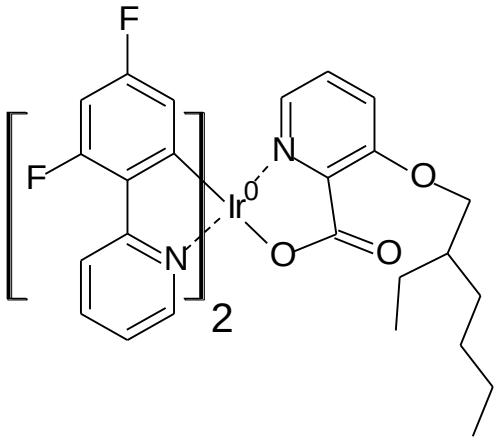

Figure 29 – Structure of IrEH.

As with FIrPic, IrEH was dispersed in TFS prior to monolith fabrication. Vinyl toluene was added to the solid mixture to achieve a set of four samples with 4 wt% IrEH and a range of TFS/VT compositions (30, 40, 50, and 60 wt%). Unlike the FIrPic samples, and despite the pre-dispersion of IrEH, these solutions failed to achieve transparency even in the liquid state. All four samples were opaque. After curing, monoliths remained opaque and the 60 wt% sample exhibited apparent crystallization visible on

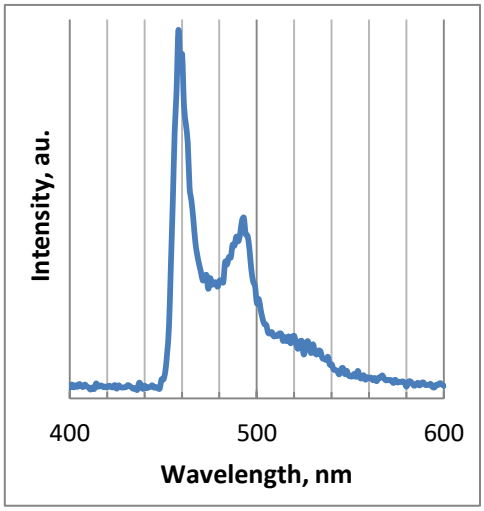

Figure 30 – Phosphorescence emission spectrum of IrEH at 77K.

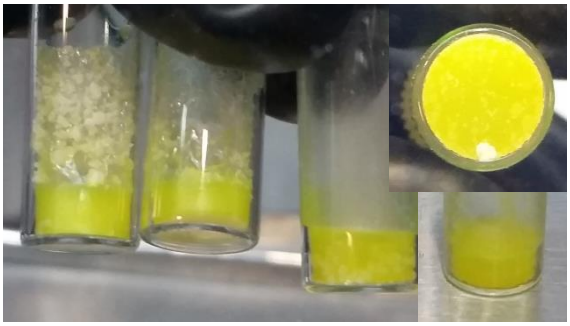

Figure 31 – A series of TFS in VT samples ranging from 30% to 60wt% (from left to right) containing 4% IrEH. A bottom view (insert) for the 60% sample is included where small inclusions of possibly crystalline IrEH can be seen.

the bottom surface. In addition all samples suffered from a foaming effect to various degrees during curing. This effect is possibly a result of phase segregation during polymerization. Figure 31 and Figure 32 show the monoliths.

With the aliphatic chain functionalization not succeeding as a dispersal mechanism, an alternative approach was needed. Iridium complexes with attached styrenyl groups were proposed as a mechanism to achieve the desired loading. These complexes would be functionalized for co-polymerization with the polymer matrix, thereby locking them into place in the final structure. The structural additions will likely not improve the solubility of the complexes in the matrix beyond the improvements of IrEH, but the inability of complexes to drift and aggregate during curing should allow for the creation of a thermodynamically unstable but kinetically locked transparent state. This would effectively lock in the initial transparent melt state achieved by the FIrPic samples.

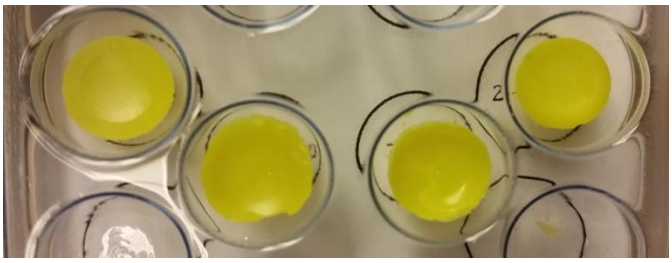

Figure 32 – Samples seen in Figure 31 after demolding and removal of foaming. TFS concentration increases from left to

Although a candidate complex for this theory was identified [Figure 25] and several synthetic pathways were explored in some detail, the focus of our triplet harvesting research has shifted to the use of TADF materials. This has largely been driven by the increasing interest in and demonstrated potential of TADF materials in other applications, which has led to a growing library of such compounds and better understanding of their underlying photophysics and design principles. In

addition, a move away from Iridium as a raw material is beneficial from both a cost and long term supply standpoint.

TADF Results

The two suggested compounds shown in Figure 26 are modified versions of literature compounds.[83,84] As with the organometallic phosphorescent dopants discussed above, the modifications were designed to improve solubility of the relevant compounds for our bulk polymerization purpose.

Each of the target compounds possess the "core and wing" structure designed to spatially separate the HOMO and LUMO orbitals and achieve minimized ΔE_{ST}. In TADF1, the outer cabazole units were synthesized as described in [Scheme 4] while the core of TADF2 was easily synthesized and purified as described in [Scheme 5] and the associated experimental. However beyond these structures synthesis of the compounds was hindered by synthetic issues. In TADF1 synthesis of the molecular core requiring the conversion of 1,3-dibromo-5,6difluorobenzene to 1,3-dicyano-4,6-difluorobenzene was unachievable despite attempts to adapt a range of published synthetic methods [Scheme 7].[83,86,87]

Scheme 7 – Three published synthetic pathways explored to cyanate 1,3-dibromo-5,6difluorobenzene.

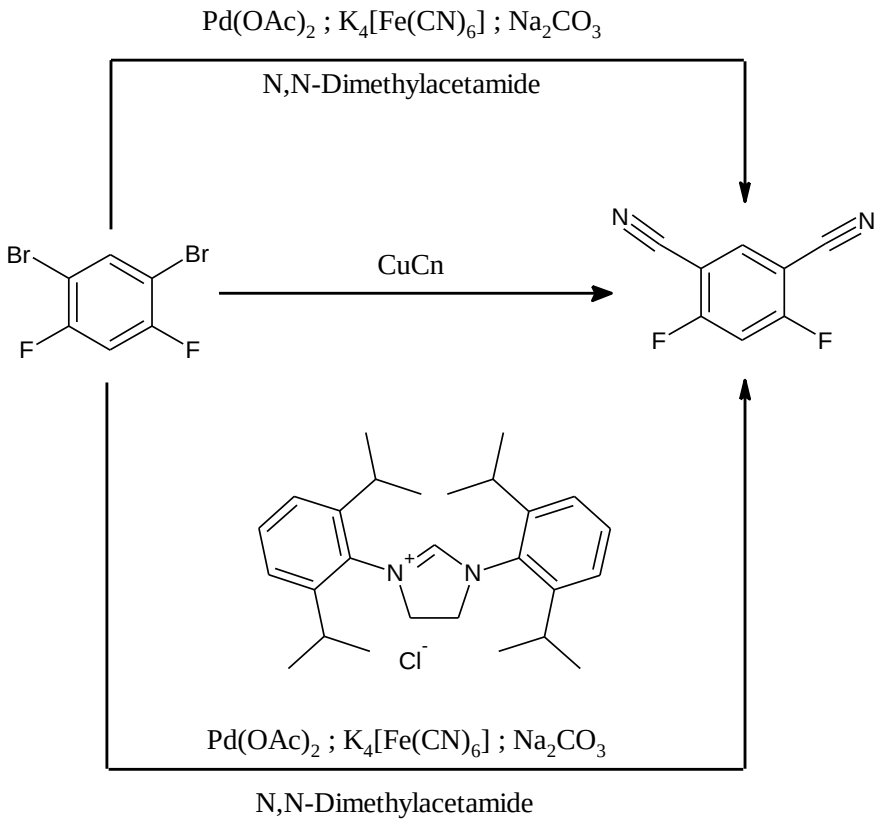

Scheme 8 – Successful synthetic pathway to acridine precursor.

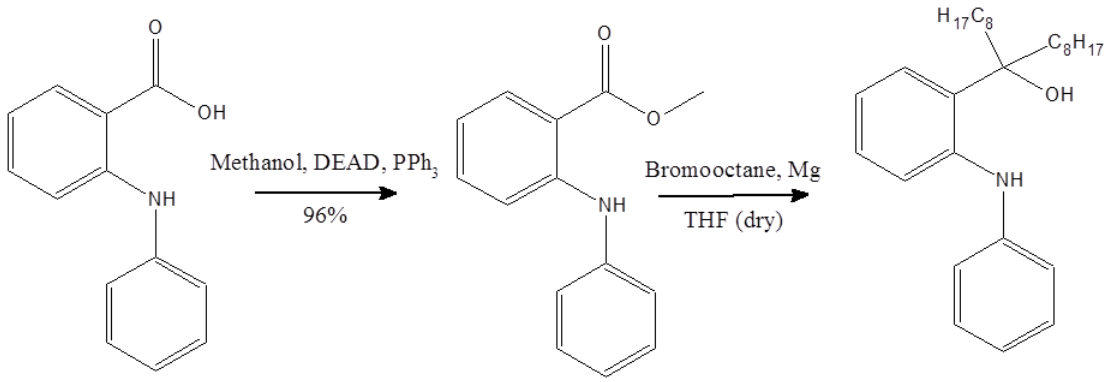

The synthesis of TADF2 encountered problems in synthesis of the outer acridine moieties. These problems were determined to be directly related to the alterations implemented to achieve higher solubility – i.e. the incorporation of longer aliphatic chains at the 9 position of the acridine. The change of of 9,9-dimethyl-9,10-dihydroacridine to 9,9-dioctyl-9,10-dihydroacridine materially affected the success of the cyclization reaction in the step immediately prior to coupling the acridine units to the central sulfone moiety. Synthesis proceeds via Grignard reaction as in Scheme 8. However, the following step, using an acid to promote condensation and cyclization [Scheme 9], fails to generate 9,9-dioctyl-9,10-dihydroacridine in any significant yield. Although a small portion can be isolated for analysis, two other primary products dominate. These unknown products are identified as S1 and S2.

Scheme 9 – Desired cyclization step.

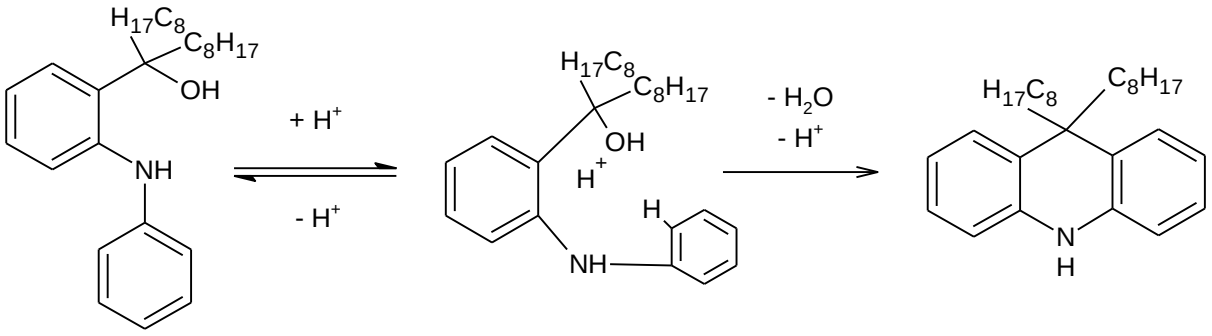

Examining the NMR spectra in Figure 33 for the three products (S1, S2, and 9,9-dioctyl-9,10-dihydroacridine) one immediately apparent clue to the identity of the major products is the integration values in the aromatic region of the spectrum. The integrations are all referenced to the 6 H peaks at the lowest chemical shift which represent the methyl protons at the ends of the

octyl chains in each molecule. For clarity, this upfield portion of the spectrum is not shown. The integration values for S1 and S2 reach 9 H, higher than the 8 H expected in the desired product. The 9 H value is consistent with the interpretation that the cyclization has failed in both cases. However based on TLC comparison to starting materials, a reaction has taken place.

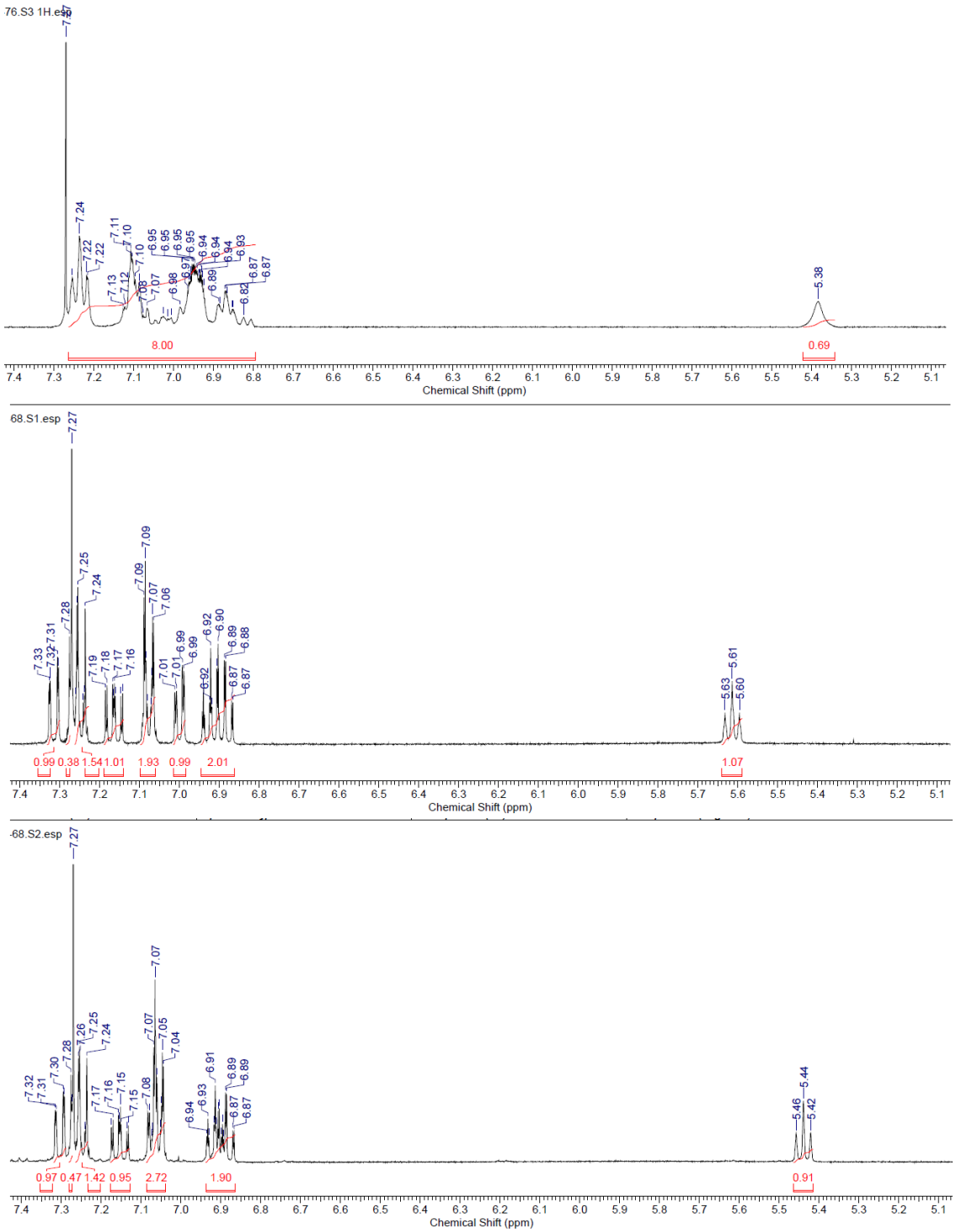

Figure 33 – NMR spectra of 9,9-dioctyl-9,10-dihydroacridine (a) and the two primary product samples, S1 and S2 (b & c respectively)

The triplets at 5.61 and 5.44 ppm in the S1 and S2 spectra indicate, from the chemical shift and splitting, the presence of a single proton in an environment not found in the 9,9-dioctyl-9,10-dihydroacridine. The only peak which corresponds in Figure 33 (a) is the broad singlet seen at 5.38 ppm which is attributed to the amine proton of the final product and here is visible as a consequence of the much higher concentration of this NMR sample. At lower concentration the peak is present as the broad hump in the baseline which can also be seen in the S1 and S2 NMR spectra at higher vertical magnification. At this point consultation of literature is instructive to suggest side reactions which may be occurring. An excellent resource is Andrew et al., which explores a range of 9 position functionalized acridines for unrelated applications in chemical sensing.[88] The variety of structures used in this context shows the broad spectrum applicability of our reaction conditions – however crucially no structure used by Andrew et al. possess an aliphatic chain longer than ethyl or a more acidic proton alpha to the eliminating hydroxyl group. From this collective information, it is deduced that the application of acid to the 2-(1-hydroxy-1-octylnonyl)-N-phenylbenzeamine primarily generates the two elimination isomers [Figure 34]. These isomers are not available to other functionalized acridines seen in the literature due to the higher acidity of the α–methylene protons in the octyl substituted compound as compared to the methyl protons in the original literature compound.

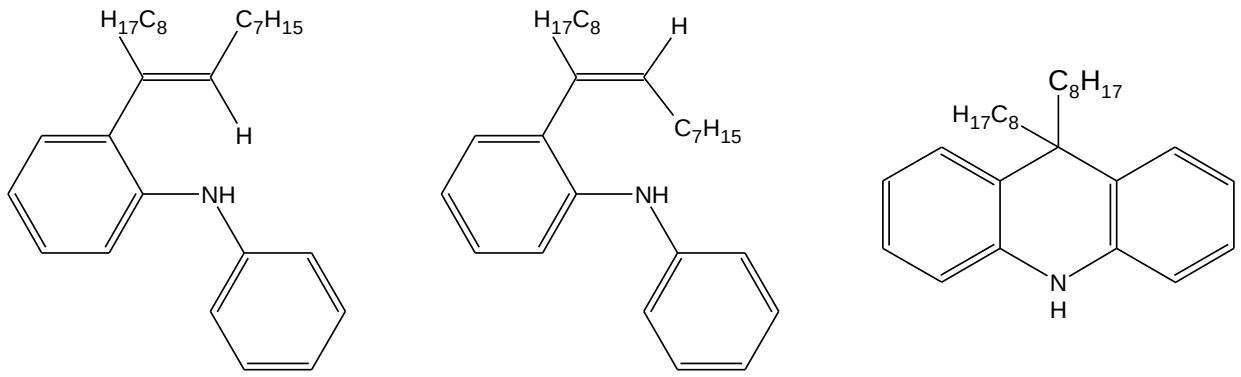

Figure 34 - Isomers resulting from attempted 9,9-dioctyl-9,10-dihydroacridine synthesis. From left to right: S1, S2, and the desired product.

Rather than engage in the time consuming search for a new synthetic approach to desired acridine target, an alternative target TADF material, known as DMT-DCz [Scheme 6] was designed. This material makes use of the carbazole units which were to comprise the outer structure of TADF1 and the successfully synthesized sulfone core of TADF2. The last step, coupling between the two components, is achieved in good yield under literature conditions and with no purification difficulties. Thus DMT-DCz exhibits none of these synthetic difficulties seen in the other target materials.

With no literature reports of our novel material, the primary tests performed on DMT-DCz were photophysical, to confirm the utility of its absorption and emission characteristics as a scintillator additive. Measurements showed absorption bands at 296 and 349 nm with emission ranging from 393 nm in toluene to 423 nm in chloroform [Figure 35]. The toluene emission is the most important – toluene is a good analogue for the molecular environment the DMT-DCz will be in in PVT based scintillators. In addition, the wavelength is in an optimal range for

pairing with the blue PMTs which are primarily used in scintillator detection. At the high loadings required for triplet capture from the matrix wavelength shifters will be critical to overcoming self-absorption and achieving usable light output from these devices. Choosing the right wavelength shifter will move the absorption color to higher wavelengths, but with a starting wavelength below 400 nm even the shifted color should be well matched to the PMT. Note that the solvatochromic 30 nm separation between the emission of toluene and chloroform which is evident to the naked eye in Figure 36 is a positive indicator of potential TADF performance. Emission sensitivity to solvent polarity is a feature of TADF molecules which results from the particular electron distribution of the charge transfer state.[51]

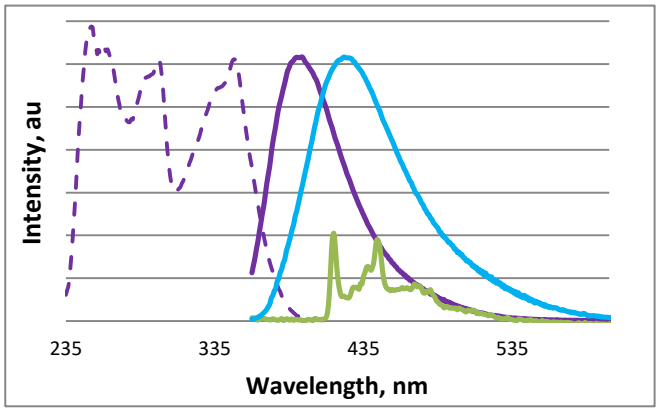

Figure 35 – Photophysical characterization of DMT-DCz in solution. Excitation in chloroform (purple, dashed), photoluminescence in toluene (purple, solid), photoluminescence in chloroform (purple), and phosphorescence emission (green) are all shown on an arbitrary intensity scale.

Figure 36 - DMT-DCz exhibits clear solvatochromism. Under UV light, the color difference from solutions in Toluene (left) to Chloroform (right) is visible to the naked eye.

Before fabricating samples however, the triplet state of the molecule in question must be confirmed. Triplet state measurements must be performed at cryogenic temperatures in air free environments to limit thermal and oxygen quenching. To achieve this, methlycyclohexane is used as a solvent because it forms an optical glass at liquid nitrogen temperatures (alternative solvents include some alcohol mixtures and methyltetrahydrofuran).

Solutions were all degassed via freeze-pump-thaw prior to measurement. By using a pulsed light source and measuring the light emission after a delay, the phosphorescence can be separated from the fluorescence of the molecule. When this is done, the phosphorescent emission, shown with the fluorescence data in Figure 35 and enlarged in Figure 37, is determined to be 415 nmFigure 26. This corresponding to a triplet energy of 2.99 eV and a ΔE_{ST} of 170 meV. These properties are in line with a TADF compound with good potential for scintillator applications.

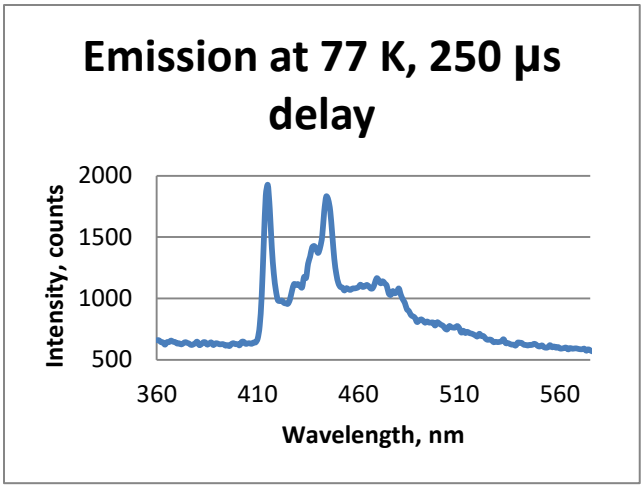

Figure 37 – Phosphorescence spectrum of DMT-DCz.

Determination of the quantum yield for DMT-DCz were made using carefully controlled concentrations and conditions to achieve comparable, qualitative absorbance and photoluminescence measurements across the solution set [Table 3].

Table 3 – Solutions of diphenylanthracene (DPA) standard and DMT-DCz prepared for determination of the DMT-DCz quantum yield. The solutions of each compound are ordered from lowest to highest concentration. The refractive index, n, of each solvent is given.

Solution ID	Solvent (n)	Concentration (mM)	Absorbance (AU)	Integrated PL (counts)
DPA 1	Cyclohexane (1.427)	7.57E-04	0.012	4494413.778
DPA 2		2.27E-03	0.026	14301001.39
DPA 3		4.54E-03	0.054	28210064.01
DMT-DCz 1	Toluene (1.497)	3.24E-07	0.008	3243107.865
DMT-DCz 2		1.08E-06	0.037	10354944.16
DMT-DCz 3		2.16E-06	0.083	20231456.1

After measurements were taken, the integrated photoluminescence intensity was plotted versus the absorbance for the series of solutions of each compound. Best fit lines were drawn for the sample and the standard. Using the slope of these lines (δ_x and δ_s respectively), the quantum yield of DMT-DCz was determined using Equation 8.

Equation 8

$$\frac{QY(X)}{QY(S)} = \frac{\delta_x}{\delta_s}\frac{n_x^2}{n_s^2}$$

Where n_x and n_s are the refractive indicies of the solvents for the sample and the standard respectively and QY(X) and QY(S) represent the quantum yield of the sample and standard respectively.

The measured quantum yield of the compound is only 44%, low for a primary dye, but not out of place among a selection of other TADF compounds in the literature.[50] As Dias et al. note, "a clear trade-off exists between the efficiency of the RISC mechanism and the electronic coupling between [] ground and excited states."[51] In other words, the low orbital overlap which results in sufficiently small ΔE_{ST} for TADF also significantly reduces fluorescent quantum yield. Clearly future work in this area will require the balancing of these factors to reach optimal performance.

With the photophysical properties showing promise, testing of compound solubility in potential matrix solutions was undertaken. A goal of achieving ~30 wt%. DMT-DCz is set as a point where significant triplet energy should be collected. This is in the range of loadings for PSD scintillators using similar principles. To limit material waste if this loading is unachievable, a range of lower loading samples were made – up to 9.8 wt% DMT-DCz. These samples all

show successful dissolution in PVT. After demolding, photoluminescence spectra of each monolith were taken to determine the emission profile. Light yield measurements show poor performance versus the standard with a flat trend across rising DMT-DCz concentration [Table 4]. Self-absorption is evident from the emission red-shifting as samples increase in DMT-DCz content. Consequently, a comparison of possible wavelength shifting compounds would be suitable prior to formulation of samples with even higher TADF content.

Table 4 - PVT/DMT-DCz sample content and light yield. Weight percentages are rounded. All samples contain 0.5 wt% Sigma Aldrich Luperox® 231 initiator. Light yields are given as a percentage of standard and have been adjusted for spectral differences.

Composition, wt%		**Light Yield, %**
Vinyl Toluene	**DMT-DCz**	**EJ-212 (Adj)**
98	1.5	39
97	3	40
95	5	40
92	7.5	40
90	9.8	37

Choosing a wavelength shifter [WLS] requires a compound with the smallest possible Stoke's shift which still minimizes self-absorption. The compound must also possess an absorption peak matched to the emission of the compound being shifted. Selecting a WLS for DMT-DCz is streamlined by realizing that the emission of 393 is exactly that of TFS used as a matrix material above. Therefore the dyes explored for TFS are potential WLS for DMT-DCz. The library of possible dyes can be expanded because the lower concentration required for WLS versus a primary dye (0.05 wt% vs >1 wt%) relaxes the solubility requirement. As a result, four dyes were chosen as potential candidates: ADS086BE, ADS129BE, TFS and Coumarin 500. Each potential WLS was incorporated into a monolith sample of 10 wt% DMT-DCz in PVT [Table 5Table 4]. All WLS demonstrated acceptable solubility, with no segregation or precipitation evident to the naked eye [Figure 38]. Measurements showed the ADS86 as the best performing WLS.

Figure 38 – Wavelength shifter test samples under UV(Top) and room (Bottom) lighting. The samples contain (from left to right) TFS, Coumarin 500, ADS086BE, and ADS129BE. The samples show excellent transparency.

Table 5 - PVT/DMT-DCz sample content and light yield. Weight percentages are rounded. All samples contain 0.5 wt% Sigma Aldrich Luperox® 231 initiator. The wavelength shifter was employed at 0.05 wt% and the compound used is listed. Light yields are given as a percentage of standard and have been adjusted for spectral differences.

Composition, wt%		**Wavelength**	**Light Yield, %**
Vinyl Toluene	**DMT-DCz**	**Shifter**	**EJ-212 (Adj)**
90	10	TFS	40
90	10	Coumarin 500	50
90	10	ADS86	56
90	10	ADS129	48

Having determined the optimal WLS, samples of higher DMT-DCz content can be explored. Monoliths of PVK and PVT containing DMT-DCz were fabricated. There exists disagreement in the literature on the triplet state of PVK, which is varyingly placed between 2.5 and 3 eV.[89–91] Unfortunately any insight into this that might be gained from using PVK as a matrix material was hindered by the failure to fabricate clear samples at high DMT-DCz loadings.

Prior work with PVK monoliths has indicated a tendency for these samples to crack during curing or cool down – limiting the ability to reproducibly form good quality samples. The high loadings of TADF material here, presuming effective solubility, should act as a plasticizer

and reduce the tendency of samples to mechanically fail. In addition we have experimented with using a PVK-co-PMMA matrix to achieve better mechanical quality in our samples and solubility for the DMT-DCz.

The samples made are described in Table 6. While preparing PMD-1 (via Route 1), there was significant difficulty achieving dissolution of DMT-DCz in the monomer melt. This necessitated the continued addition of MMA to the mixture above the originally intended 10 wt% to achieve a homogenous mixture at the final wt% shown in Table 6. It is possible that more patience in the melting/vortexing cycle could have resulted in a homogenous mixture without the additional MMA, however in any case the sample suffered severe segregation during curing. By the finish of the curing cycle the sample was entirely opaque as clear precipitation occurred.

Table 6 - PVK/PMMA/DMT-DCz sample content. Weight percentages are rounded. All samples contain 0.05 wt% ADS086BE as a wavelength shifter and 0.5 wt% Luperox® 231 initiator.

Sample ID	NVK, wt%	MMA, wt%	DMT-DCz, wt%
PMD-1	50	25	25
PMD-2	38	38	23

PMD-2 was prepared via Route 2, and improvements in the initial mixing were immediately apparent. A homogenous mixture was achieved purely through melting the solid mixture which had been created. MMA was added with the aim of maintaining transparency in the final sample. Despite the improvement, the sample was not transparent during or after curing.

Results with a PVT matrix were much more promising. A monolith of 29 wt% DMT-DCz in PVT was fabricated and characterized [Figure 39]. The TADF dye dissolves easily in the PVT – requiring no additional effort above that used for the lower concentrations even at this high loading. The final monolith is transparent and shows no apparent precipitation or segregation of TADF material to the naked eye.

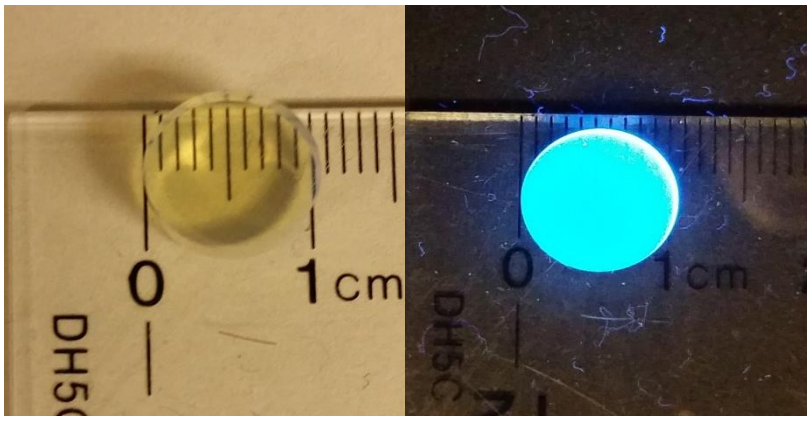

Figure 39 – Sample 3-97 (4 mm thick) under room (right) and UV illumination (left).

Light yield testing on the monolith showed poor results as compared to the EJ-212 standard, with no evidence of improved light yield resulting from harvesting of triplet excitons. The likely cause is the lower triplet energy of PVT compared to the TADF material which leads to back transfer of excitons and reduces the opportunity for TADF up-conversion to emissive singlet states. While the PVT demonstrated the high solubility of the DMT-DCz and showed at least some scintillation capability (related, presumably, to its fluorescence properties although constrained by its comparatively low quantum yield), to achieve a true improvement the use of a matrix material with a higher T_1 state is required.

Conclusions and Future Work

The results presented here demonstrate a novel TADF candidate compound, DMT-DCz, with high solubility in the correct matrix material and the potential to add to the performance of plastic scintillators through triplet harvesting. This represents an important step forward in moving away from expensive, rare metals in this area of application – allowing for the realization of similar results through a different mechanism using cheap, high solubility, and all organic TADF compounds.

In DMT-DCz, the solvatochromism observed and phosphorescence/fluorescence measurements taken point to a ΔE_{ST} within the range of TADF processes. The high singlet state, with an emission at 393 nm in toluene makes this compound ideally suited for applications in scintillators. And when paired with a high efficiency wavelength shifter the emission remains in a suitable for pairing with both PMTs and solid state detectors. In addition, the successful incorporation of DMT-DCz at 30 wt% in PVT demonstrates that with the correct matrix choices a triplet-harvesting dopant level of loading is achievable. Unfortunately similar loadings were not realized with a PVK based matrix.

In future work, higher performance will require the use of higher triplet state polymer matrices. In some cases assessing the triplet state of these polymers can be difficult with the tools available, however potential candidates such a poly(methyl methacrylate) and polystyrene are worth exploration. Another route may be the synthesis of custom monomers for fabrication of

new polymer matrices. For example, a silicon cored matrix material such as the ultra-high band gap materials shown by Ren et al. offers potential opportunities.[92]

VI. Summary

The importance of this work is driven by the necessity for wide scale deployment of cheap, rugged, and effective detectors to counter potential radiological threats across a massive search space which encompasses virtually all trade entering the United States. The potential radiological/nuclear threats presented by potential adversaries are clear; as are the economic costs associated with time consuming or destructive analysis. Current technologies do not meet the needs of the security community. Although plastics offer a range of benefits, their overall gamma light yield performance remains subpar.

To address this, we have sought to improve gamma scintillation light yield while maintaining the robust nature, ease of fabrication, and scalability which are the hallmarks of plastic scintillators. This project has undertaken a two pronged approach to push performance beyond the current commercial benchmarks. We have identified, synthesized, and characterized novel polymer systems and additives which achieve these ends. Applying expertise in photoactive organic materials, we demonstrated a successful approach to meeting this challenge and point the way forward to further improvements and better technology solutions.

The project began with the successful identification and synthesis of potential fluorescent matrix materials to replace PVT in the scintillator system. These matrices were designed with particular goals including emission wavelength and melting point. Following synthesis, they were paired with both commercial and custom fluors as dictated by their properties and easily cured into scintillator monoliths through a melt curing process under nitrogen. The speed and economy of the curing process, as well as the mechanical properties and machinability of the samples demonstrated by their successful grinding and polishing, demonstrates that our materials maintain the desirable properties of plastic scintillators. In addition, the performance of the TFS/VT system, our most promising result, shows a 12,700 ph/MeV light yield. This combination of plastic scintillator traits with a significant light yield improvement demonstrates the utility of OLED materials in general and fluorenyl materials in particular for improving plastic scintillator technology. Furthermore, the success of the system when used with SiPMs and the substantial outperformance of the green standard technology opens up a new range of uses for the materials studied. These applications include pairing with new types of detectors, making use of the higher green sensitivities available in solid state detectors, and better compatibility with light pipping required in certain contexts.

The second prong of our approach, the use of novel dopants, has focused on the potential of triplet harvesting to open up new radiative pathways for improved light yield. The initial exploration of Iridium based materials was abandoned in favor of realizing similar results through a different mechanism using cheap, high solubility, and all organic TADF compounds. The results presented here demonstrate a novel TADF candidate compound, DMT-DCz, with high solubility and the potential to add to the performance of plastic scintillators through triplet harvesting. The photophysics and solubility of DMT-DCz represents a proof of concept of the

theory behind this work. While initial light yields are lower than desired, a clear path forward is proposed to incorporate the material designed into higher triplet energy polymers and allow full utilization of the available energy. In addition, the explosive growth of organic photoelectric materials and rapidly evolution of TADF understanding offers real opportunities to even further improve on these results. It is our hope that this work will lead not only to a short term improvement in scintillator performance, but to the opening of new avenues of research and new materials entering a field which has seen little fundamental change in 50 years. The future of plastic scintillators is bright.

VII. References

[1] "Don't Fear the Dirty Bomb," can be found under http://warontherocks.com/2015/10/dont-fear-the-dirty-bomb/, **2015**.

[2] "NRC: Fact Sheet on Dirty Bombs," can be found under http://www.nrc.gov/reading-rm/doc-collections/fact-sheets/fs-dirty-bombs.html, **n.d.**

[3] "Port Industry Statistics - Port Industry Information - AAPA," can be found under http://www.aapa-ports.org/Industry/content.cfm?ItemNumber=900, **n.d.**

[4] "Port of Long Beach - Yearly TEUs," can be found under http://www.polb.com/economics/stats/yearly_teus.asp, **n.d.**

[5] E. R. Siciliano, J. H. Ely, R. T. Kouzes, B. D. Milbrath, J. E. Schweppe, D. C. Stromswold, *Nucl. Instrum. Methods Phys. Res. Sect. Accel. Spectrometers Detect. Assoc. Equip.* **2005**, *550*, 647.

[6] G. H. V. Bertrand, M. Hamel, S. Normand, F. Sguerra, *Nucl. Instrum. Methods Phys. Res. Sect. Accel. Spectrometers Detect. Assoc. Equip.* **2015**, *776*, 114.

[7] R. J. Kloeppingt, *IEEE Trans. Nucl. Sci.* **1975**, *22*, 81.

[8] E. Tupitsyn, P. Bhattacharya, E. Rowe, L. Matei, Y. Cui, V. Buliga, M. Groza, B. Wiggins, A. Burger, A. Stowe, *J. Cryst. Growth* **2014**, *393*, 23.

[9] J. E. McMillan, A. J. Cole, A. Kirby, E. Marsden, *J. Phys. Conf. Ser.* **2015**, *620*, 012011.

[10] H. P. Chou, C. Y. Horng, *Nucl. Instrum. Methods Phys. Res. Sect. Accel. Spectrometers Detect. Assoc. Equip.* **1993**, *328*, 522.

[11] A. N. Mabe, M. J. Urffer, D. Penumadu, G. K. Schweitzer, L. F. Miller, *Radiat. Meas.* **2014**, *66*, 5.

[12] H. A. Yemam, A. Mahl, U. Koldemir, T. Remedes, S. Parkin, U. Greife, A. Sellinger, *Sci. Rep.* **2015**, *5*, 13401.

[13] Z. H. Cho, C. M. Tsai, L. A. Eriksson, *IEEE Trans. Nucl. Sci.* **1975**, *22*, 72.

[14] M. Hamel, G. Turk, S. Darbon, S. Normand, *IEEE Trans. Nucl. Sci.* **2012**, *59*, 1268.

[15] J. Dannin, S. R. Sandler, B. Baum, *Int. J. Appl. Radiat. Isot.* **1965**, *16*, 589.

[16] O. H. Nestor, C. Y. Huang, *IEEE Trans. Nucl. Sci.* **1975**, *22*, 68.

[17] B. L. Rupert, N. J. Cherepy, B. W. Sturm, R. D. Sanner, S. A. Payne, *EPL Europhys. Lett.* **2012**, *97*, 22002.

[18] W. Cai, Q. Chen, N. Cherepy, A. Dooraghi, D. Kishpaugh, A. Chatziioannou, S. Payne, W. Xiang, Q. Pei, *J. Mater. Chem. C* **2013**, *1*, 1970.

[19] C. Liu, T. J. Hajagos, D. Kishpaugh, Y. Jin, W. Hu, Q. Chen, Q. Pei, *Adv. Funct. Mater.* **2015**, *25*, 4607.

[20] Y. Jin, D. Kishpaugh, C. Liu, T. J. Hajagos, Q. Chen, L. Li, Y. Chen, Q. Pei, *J. Mater. Chem. C* **2016**, *4*, 3654.

[21] R. Hofstadter, *Phys. Rev.* **1948**, *74*, 100.

[22] M. Nikl, *Meas. Sci. Technol.* **2006**, *17*, R37.

[23] **2009**.

[24] A. J. Bird, T. Carter, A. J. Dean, D. Ramsden, B. M. Swinyard, *IEEE Trans. Nucl. Sci.* **1993**, *40*, 395.

[25] K. Sreebunpeng, W. Chewpraditkul, M. Nikl, J. A. Mares, *Procedia Eng.* **2012**, *32*, 577.

[26] M. Moszyński, M. Kapusta, D. Wolski, W. Klamra, B. Cederwall, *Nucl. Instrum. Methods Phys. Res. Sect. Accel. Spectrometers Detect. Assoc. Equip.* **1998**, *404*, 157.

[27] E. V. D. van Loef, P. Dorenbos, C. W. E. van Eijk, K. W. Krämer, H. U. Güdel, *Nucl. Instrum. Methods Phys. Res. Sect. Accel. Spectrometers Detect. Assoc. Equip.* **2002**, *486*, 254.

[28] S. R. Sandler, K. C. Tsou, *Int. J. Appl. Radiat. Isot.* **1964**, *15*, 419.

[29] G. I. Britvich, V. G. Vasil'chenko, V. G. Lapshin, A. S. Solov'ev, *Instrum. Exp. Tech.* **2000**, *43*, 36.

[30] S. Niese, *J. Radioanal. Nucl. Chem.* **1999**, *241*, 499.

[31] "EJ-301," can be found under http://www.eljentechnology.com/index.php/products/liquid-scintillators/71-ej-301, **n.d.**

[32] J. B. Birks, *The Theory and Practice of Scintillation Counting*, **n.d.**

[33] "EJ-200," can be found under http://www.eljentechnology.com/index.php/products/plastic-scintillators/48-ej-200, **n.d.**

[34] R. C. Powell, *J. Chem. Phys.* **1971**, *55*, 1871.

[35] J. Guillet, *Polymer Photophysics and Photochemistry: An Introduction to the Study of Photoprocesses in Macromolecules*, Cambridge University Press, Cambridge [Cambridgeshire]; New York, **1985**.

[36] *J. Appl. Phys.* **2007**, *102*, 114504.

[37] C.-J. Chiang, A. Kimyonok, M. K. Etherington, G. C. Griffiths, V. Jankus, F. Turksoy, A. P. Monkman, *Adv. Funct. Mater.* **2013**, *23*, 739.

[38] H. Yersin, *Highly Efficient OLEDs with Phosphorescent Materials*, Wiley-VCH, Weinheim, **2008**.

[39] F. B. Dias, K. N. Bourdakos, V. Jankus, K. C. Moss, K. T. Kamtekar, V. Bhalla, J. Santos, M. R. Bryce, A. P. Monkman, *Adv. Mater.* **2013**, *25*, 3707.

[40] B. S. Kim, K. S. Yook, J. Y. Lee, *Sci. Rep.* **2014**, *4*, 6019.

[41] M. Taneda, K. Shizu, H. Tanaka, C. Adachi, *Chem. Commun.* **2015**, *51*, 5028.

[42] W.-L. Yu, J. Pei, W. Huang, A. J. Heeger, *Adv. Mater.* **2000**, *12*, 828.

[43] C. Tang, F. Liu, Y.-J. Xia, J. Lin, L.-H. Xie, G.-Y. Zhong, Q.-L. Fan, W. Huang, *Org. Electron.* **2006**, *7*, 155.

[44] K.-S. Kim, Y.-M. Jeon, J.-W. Kim, C.-W. Lee, M.-S. Gong, *Org. Electron.* **2008**, *9*, 797.

[45] C.-G. Zhen, Z.-K. Chen, Q.-D. Liu, Y.-F. Dai, R. Y. C. Shin, S.-Y. Chang, J. Kieffer, *Adv. Mater.* **2009**, *21*, 2425.

[46] S. Lamansky, R. C. Kwong, M. Nugent, P. I. Djurovich, M. E. Thompson, *Org. Electron.* **2001**, *2*, 53.

[47] Q. Zhang, H. Kuwabara, W. J. Potscavage, S. Huang, Y. Hatae, T. Shibata, C. Adachi, *J. Am. Chem. Soc.* **2014**, *136*, 18070.

[48] A. F. Scott, *Survey of Progress in Chemistry*, Elsevier, **2013**.

[49] S. Zhang, W. Li, L. Yao, Y. Pan, F. Shen, R. Xiao, B. Yang, Y. Ma, *Chem. Commun.* **2013**, *49*, 11302.

[50] Y. Tao, K. Yuan, T. Chen, P. Xu, H. Li, R. Chen, C. Zheng, L. Zhang, W. Huang, *Adv. Mater.* **2014**, *26*, 7931.

[51] F. B. Dias, T. J. Penfold, A. P. Monkman, *Methods Appl. Fluoresc.* **2017**, *5*, 012001.

[52] S. Majewski, M. Bowen, C. Zorn, K. Johnson, V. Hagopian, J. Thomaston, H. Wahl, *Nucl. Instrum. Methods Phys. Res. Sect. Accel. Spectrometers Detect. Assoc. Equip.* **1989**, *281*, 500.

[53] W. Busjan, A. Dannemann, U. Holm, T. Neumann, V. Schlottmann, K. Wick, *Nucl. Phys. B - Proc. Suppl.* **1993**, *32*, 392.

[54] E. Reichmanis, J. H. O'Donnell, American Chemical Society, Division of Polymer Chemistry, Royal Australian Chemical Institute, Polymer Division, Eds. , *The Effects of Radiation on High-Technology Polymers: Developed from a Workshop Sponsored by the Division of Polymer Chemistry, Inc., of the American Chemical Society and the Polymer Division of the Royal Australian Chemical Institute, Queensland, Australia, August 16-19, 1987*, American Chemical Society, Washington, DC, **1989**.

[55] A. D. Bross, A. Pla-Dalmau, *IEEE Trans. Nucl. Sci.* **1992**, *39*, 1199.

[56] L. Torrisi, *Radiat. Phys. Chem.* **2002**, *63*, 89.

[57] Z. Li, W. Chong, H. Yuekun, Z. Xiaojian, S. Feng, S. Zhijia, W. Jinjie, A. Zhenghua, Z. Yuda, Z. Ziping, W. Yifang, *Nucl. Instrum. Methods Phys. Res. Sect. Accel. Spectrometers Detect. Assoc. Equip.* **2005**, *552*, 449.

[58] W. L. Buck, R. K. Swank, *United States Patent: 2824841 - Scintillator Composition for Counters and Methods of Making*, **1953**, 2824841.

[59] M. Hyman, *United States Patent: 2710284 - Fluorescent Chemical Scintillators*, **1955**, 2710284.

[60] R. Kretz, L. Hosch, *United States Patent: 3457180*, **1969**, 3457180.

[61] T. Shimizu, JP, J. Nakagawa, JP, *United States Patent: 4495084 - Plastic Scintillator*, **1985**, 4495084.

[62] J. K. Walker, J. R. Tymianski, *United States Patent: 5420959 - High Efficiency, High Resolution, Real-Time Radiographic Imaging System*, **1995**, 5420959.

[63] A. D. Bross, K. L. Mellott, A. Pla-Dalmau, *United States Patent: 7067079 - Extruded Plastic Scintillator Including Inorganic Powders*, **2006**, 7067079.

[64] C. Liao, H. Yang, *Nucl. Instrum. Methods Phys. Res. Sect. Accel. Spectrometers Detect. Assoc. Equip.* **2015**, *789*, 150.

[65] "NIST: X-Ray Mass Attenuation Coef. - Plastic Scintillator," can be found under http://physics.nist.gov/PhysRefData/XrayMassCoef/ComTab/vinyl.html, **n.d.**

[66] G. F. Knoll, *G. F. Knoll's Radiation Detection 3rd (Third) edition(Radiation Detection and Measurement [Hardcover])(2000)*, Wiley, **n.d.**

[67] A. Burger, E. Rowe, M. Groza, K. Morales Figueroa, N. J. Cherepy, P. R. Beck, S. Hunter, S. A. Payne, *Appl. Phys. Lett.* **2015**, *107*, 143505.

[68] I. B. Berlman, *Handbook of Fluorescence Spectra of Aromatic Molecules*, Academic Press, New York, **1971**.

[69] T. Ito, S. Suzuki, J. Kido, *Polym. Adv. Technol.* **2005**, *16*, 480.

[70] C. Ulbricht, C. R. Becer, A. Winter, D. Veldman, U. S. Schubert, *Macromol. Rapid Commun.* **2008**, *29*, 1919.

[71] Y. You, S. H. Kim, H. K. Jung, S. Y. Park, *Macromolecules* **2006**, *39*, 349.

[72] X. Wang, K. Ogino, K. Tanaka, H. Usui, *IEEE J. Sel. Top. Quantum Electron.* **2004**, *10*, 121.

[73] M. Thompson, *MRS Bull.* **2007**, *32*, 694.

[74] M. A. Baldo, D. F. O'Brien, Y. You, A. Shoustikov, S. Sibley, M. E. Thompson, S. R. Forrest, *Nature* **1998**, *395*, 151.

[75] C. Ulbricht, B. Beyer, C. Friebe, A. Winter, U. S. Schubert, *Adv. Mater.* **2009**, *21*, 4418.

[76] J. Partee, E. L. Frankevich, B. Uhlhorn, J. Shinar, Y. Ding, T. J. Barton, *Phys. Rev. Lett.* **1999**, *82*, 3673.

[77] Q. Zhang, Q. Zhou, Y. Cheng, L. Wang, D. Ma, X. Jing, F. Wang, *Adv. Mater.* **2004**, *16*, 432.

[78] W. Li, D. Liu, F. Shen, D. Ma, Z. Wang, T. Feng, Y. Xu, B. Yang, Y. Ma, *Adv. Funct. Mater.* **2012**, *22*, 2797.

[79] H. Uoyama, K. Goushi, K. Shizu, H. Nomura, C. Adachi, *Nature* **2012**, *492*, 234.

[80] W. Li, Y. Pan, R. Xiao, Q. Peng, S. Zhang, D. Ma, F. Li, F. Shen, Y. Wang, B. Yang, Y. Ma, *Adv. Funct. Mater.* **2014**, *24*, 1609.

[81] Y. Pan, W. Li, S. Zhang, L. Yao, C. Gu, H. Xu, B. Yang, Y. Ma, *Adv. Opt. Mater.* **2014**, *2*, 510.

[82] J. C. Deaton, S. C. Switalski, D. Y. Kondakov, R. H. Young, T. D. Pawlik, D. J. Giesen, S. B. Harkins, A. J. M. Miller, S. F. Mickenberg, J. C. Peters, *J. Am. Chem. Soc.* **2010**, *132*, 9499.

[83] Y. J. Cho, S. K. Jeon, B. D. Chin, E. Yu, J. Y. Lee, *Angew. Chem.* **2015**, *127*, 5290.

[84] I. Lee, J. Y. Lee, *Org. Electron.* **2016**, *29*, 160.

[85] E. Baranoff, B. F. E. Curchod, *Dalton Trans* **2015**, *44*, 8318.

[86] J. Zanon, A. Klapars, S. L. Buchwald, *J. Am. Chem. Soc.* **2003**, *125*, 2890.

[87] Z. Xu, Y. Xiao, H. Ding, C. Cao, H. Li, G. Pang, Y. Shi, *Synthesis* **2015**, *47*, 1560.

[88] T. L. Andrew, T. M. Swager, *J. Org. Chem.* **2011**, *76*, 2976.

[89] R. D. Burkhart, *Macromolecules* **1976**, *9*, 234.

[90] G. Rippen, G. Kaufmann, W. Klöpffer, *Chem. Phys.* **1980**, *52*, 165.

[91] A. van Dijken, J. J. A. M. Bastiaansen, N. M. M. Kiggen, B. M. W. Langeveld, C. Rothe, A. Monkman, I. Bach, P. Stössel, K. Brunner, *J. Am. Chem. Soc.* **2004**, *126*, 7718.

[92] X. Ren, J. Li, R. J. Holmes, P. I. Djurovich, S. R. Forrest, M. E. Thompson, *Chem. Mater.* **2004**, *16*, 4743.